# A NUMERICAL INVESTIGATION OF THE SHELF SLOPE IN THE SCALING FOR UPWELLING OVER SUBMARINE CANYONS

by

Tara Howatt

A THESIS SUBMITTED IN PARTIAL FULFILLMENT OF THE REQUIREMENTS FOR THE DEGREE OF

BACHELOR OF SCIENCE (HONOURS)

in

THE FACULTY OF SCIENCE

(Oceanography and Geophysics)

This thesis conforms to the required standard

---

Supervisor

UNIVERSITY OF BRITISH COLUMBIA

(Vancouver)

MARCH 2012

# Abstract

Submarine canyons are known regions of enhanced upwelling. Previous studies have looked into the dynamics of the upwelling and recently a scaling system by *Allen and Hickey* [2010] has been developed. A closer look into this scaling has shown that the continental shelf slope surrounding the canyon plays a role and needs to be included in the scaling. The slope plays a role in the depth of upwelling and the upwelling flux because the slope will create a back pressure restricting the flow from moving further up the shelf. This thesis will discuss the determination of a non-dimensional number to characterize the shelf slope in these upwelling quantities. A numerical model will be used to test the new scaling and to assist in finding a relation between the shelf slope and the depth of upwelling and the upwelling flux. A non-dimensional number to take into account the effect of the shelf slope has been found; however, further research is required for a physical explanation of the form of this number. Looking at the results from the model, relationships between the slope, stratification, Coriolis parameter and upwelling depth and flux can also be made, where a flatter slope, low stratification, and a low Coriolis parameter will have the greatest upwelling response.

# Contents

# List of Figures

# List of Tables

# List of Appendices

# Acknowledgments

I would like to first thank my supervisor Susan Allen, who provided much guidance along the way and made the time to meet with me every week. I would like to thank Jordan Dawe for showing me how to use the MITgcm model and Westgrid and also for his patience while I was learning. On that note I would also like to thank those from MIT who created and work on the MITgcm model which I used for my data; and to Westgrid which allowed me to run more cases than would have otherwise been possible on my own computer. And lastly, thank-you to the undergraduate thesis supervisors Erin Lane and Elspeth Barnes who supported each of us as we struggled to complete our theses.

# 1 Introduction

Submarine canyons are found along the continental shelf and enhance the upwelling in that region. A modeling study by *Kämpf* [2010] shows that the presence of submarine canyons in the eastern Great Australian Bight can increase the volume flux of water onto the shelf by a factor of 3.5. Upwelling is significant for bringing nutrient rich water from depth onto the continental shelf allowing these regions to be biologically active [*Allen et al.*, 2001].

A scaling of upwelling over submarine canyons has been developed by *Allen and Hickey* [2010]. The quantities scaled included the depth of upwelling, the flux of water upwelled onto the shelf, and the deep water stretching. A number for determining the presence of a shelf break eddy has also been developed using a scaling method. A numerical investigation of a canyon in a laboratory tank, with a diameter of one meter, indicated that this scaling can represent the upwelling fairly accurately; however, there is still need for improvement. The deep water stretching scaling deviated most from the observed values and the model used in the numerical investigation produced no shelf break eddies; thus these scales will not be explored further in this paper.

This paper will focus on investigating the influence of the continental shelf slope on an upwelling event and investigate how to fit it into the scaling of the upwelling depth and the flux of water onto the shelf. Motivation for examining the shelf slope came upon by looking into the scaling system developed by *Allen and Hickey* [2010] for the depth of upwelling and flux of water onto the shelf. Figure 1 shows that variations in the shelf slope produced results that deviated from the line of best fit and thus does not follow the proposed scaling. It is important to include the shelf slope in the scaling because many continental regions have a slope and that will make this scaling more applicable to real canyon scenarios.

In section 2 a background of the upwelling over submarine canyons will be discussed as well as the initial scaling system. Section 3 includes the methodology of the experiment and a brief description on the approach of adding the effect of the shelf slope in the scaling. Section 4 will include the results of the numerical model and a comparison with the original scales by *Allen and Hickey* [2010]. Section 5 will include the new scaling approach in more detail. Section 6 will include a verification of the new scales using the data from MITgcm. Section 7 will be a discussion of the results and how the new scaling better represents the upwelling over submarine canyons.

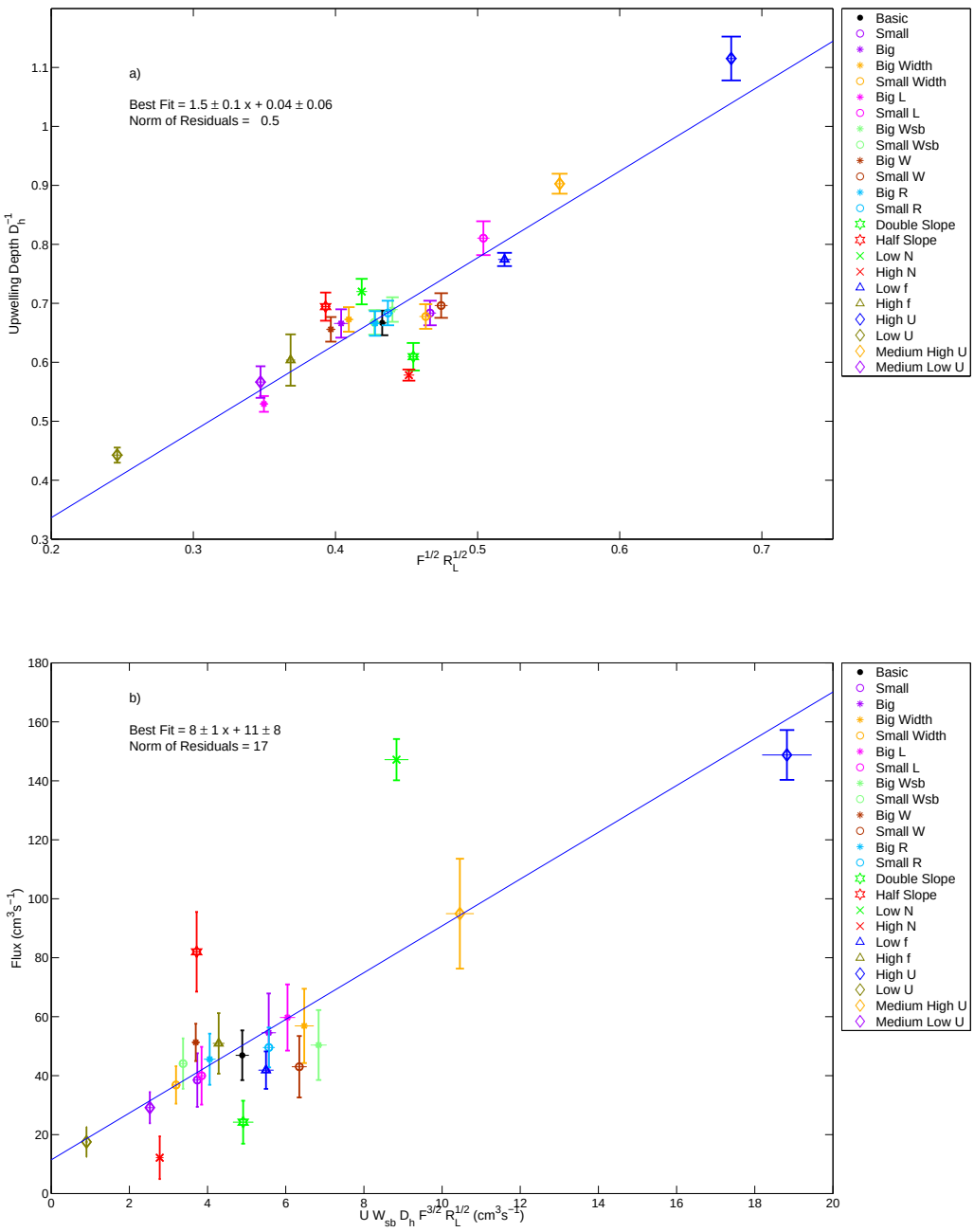


Figure 1: The original scaling system of *Allen and Hickey* [2010] for a) the depth of upwelling and b) the upwelling flux. The different dots represent the different canyon cases which varied the geometry of the canyon, the stratification,$N$; the Coriolis parameter, $f$; and the $U$ velocity upstream of the canyon. The variations in slope are shown by the red and green stars and are off the line of best fit. The x in the best fit refers to the x-axis. The norm of residuals is normalized to the x-axis.

# 2 Background

## 2.1 Upwelling over Submarine Canyons

### 2.1.1 Phases of Upwelling

There are three phases to an upwelling event: an initial transient phase, a near steady advection dominated phase, and a relaxation phase [*Allen and Durrieu de Madron*, 2009]. The initial transient phase is a time dependent response as the flow along the shelf-break increases and can be explained by linear dynamics [*Allen*, 1996]. The advection dominated phase is a response to when the shelf-break flow is steady, this phase is non-linear and a system of scales will be examined further in this paper. The relaxation phase occurs when the shelf-break flow decreases.

### 2.1.2 Components of Flow Over Canyons

Geostrophic flows have zero horizontal divergence and are forced to follow isobaths [*Allen and Durrieu de Madron*, 2009]. This being the case the flow must be ageostrophic in order to have upwelling. Some conditions for vertical water movement include large frictional forces, the importance of time dependence, or advection dominated flow [*Allen*, 2004]. Which of these actually contributes to the upwelling depends on the timing and the phase of upwelling.

There are different layers to be considered when looking at canyon upwelling: the surface flow, the upwelling current, and the deep flow [*Allen*, 2004] (Figure 2). The surface flow goes right over the canyon because it is only weakly affected by the canyon [*Allen*, 2004]. The rim depth eddy can be generated by the stretching of the water column as the flow crosses the canyon just above the canyon rim [*Allen et al.*, 2001]. The upwelling current is water that flows into the canyon and is upwelled onto the shelf [*Allen*, 2004]. The surface flow crossing the canyon is in balance with a pressure gradient at the rim depth and drives the upwelling within the canyon [*Freeland and Denman*, 1982]. There is stronger upwelling closer to shelf-break depth and weaker upwelling lower in the canyon which causes a stretching of the water column at depth. The deep flow has a cyclonic vorticity due to this stretching of the water column [*Allen*, 2004].

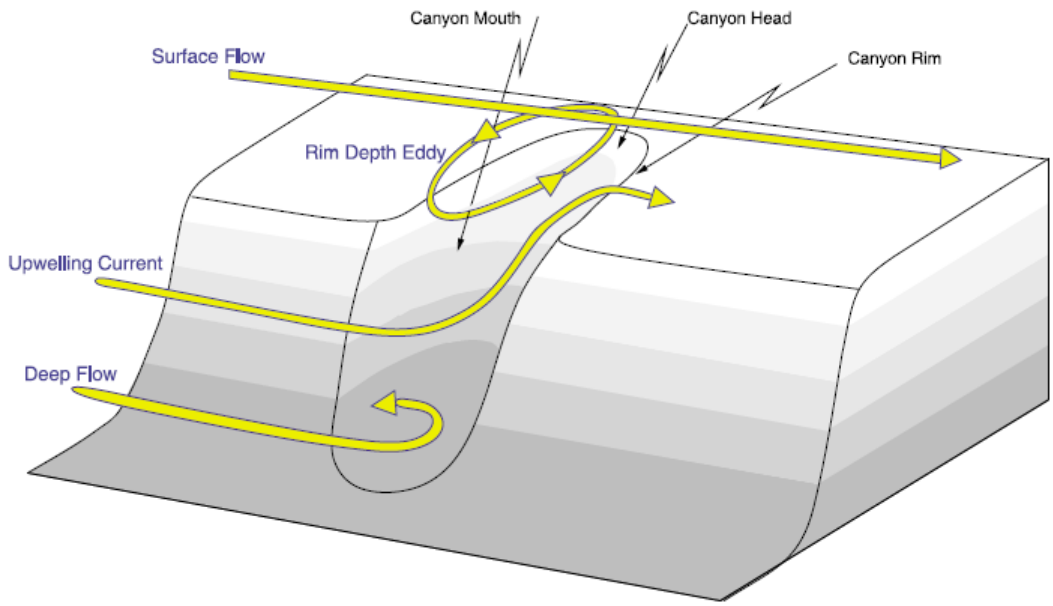


Figure 2: Schematic of flow over a submarine canyon (from *Allen and Hickey* [2010]).

## 2.2 Initial Scaling of Upwelling Over Submarine Canyons

### 2.2.1 Assumptions of the Scaling

A scaling system was developed by *Allen and Hickey* [2010]. Assumptions of the scaling include: weak to moderate, uniform incoming flow; uniform stratification near the rim depth; a shallow shelf break depth; that the canyon is deep, narrow, has steep walls and does not cut too close to the coast; and that the canyon has a regular shape at the upstream corner.

### 2.2.2 Parameters in the Scaling

The parameters used in the scaling for upwelling over submarine canyons include the along isobath velocity upstream of the canyon, $U$; the Coriolis parameter, $f$; the stratification given by the Brunt-Väisälä buoyancy frequency, $N$; the length of the canyon, $L$; the width of the canyon at half the canyon length, $W$; the width of the canyon at the shelf break, $W_{sb}$; the radius of curvature of the canyon, $R$; and the slope of the continental shelf, $s$. Figure 3 shows the canyon geometry with some of these scales drawn on which are used in the scaling described below.

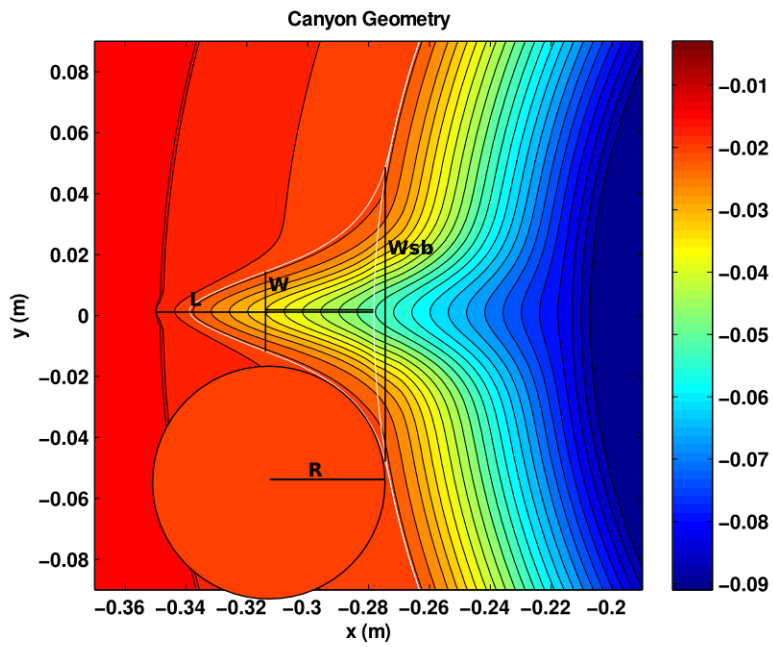


Figure 3: The geometry of the canyon is shown. The white contours represent the 0.02 m shelf-break depth. $W_{sb}$ is the shelf break width, $W$ is the width of the canyon, $L$ is the length of the canyon from the shelf break width to the head of the canyon, and $R$ is the radius of curvature of the canyon.

Other scales which are referred to are the depth to the head of the canyon, $H_h$, and the depth to the shelf break, $H_s$.

Some non-dimensional numbers used in the scaling include two Rossby numbers, $Ro = U/fR$ and $U/fW$, which determines whether the flow will follow the isobaths or cross over the canyon and drive upwelling; a function $F$ which changes $U$ velocities along isobaths to $V$ velocities across isobaths, $F = c_1 Ro/(c_2 + Ro)$ where $c_1$ and $c_2$ are constants taken to be 1 and 0.9 respectively [*Allen and Hickey*, 2010]; another Rossby number, $R_L = U/fL$; and a depth scale $D_h = fL/N$.

### 2.2.3 Scaling of the Upwelling Depth

The depth of upwelling is the depth below the head at which the deepest water arrives on the shelf. The scaling for the upwelling depth was done by estimating the strength of the flow crossing the canyon and determining the resulting pressure gradient [*Allen and Hickey*, 2010]. From this the deformation of the density field is found and by balancing the pressure gradients at the head and mouth of the canyon allows for the determination

of the depth of upwelling [*Allen and Hickey*, 2010]. The scaling for the depth of upwelling is as follows:

$$Z = \frac{fULF}{N^2} = D_h(FR_L)^{1/2} \tag{1}$$

where $Z$ is the upwelling depth, $f$ is the Coriolis parameter, $U$ is the velocity upstream of the canyon, $L$ is the length of the canyon, $F = c_1 Ro/(c_2 + Ro)$ is a function used to relate velocities $U$ and $V$ (the radially outward velocity) as flow crosses the canyon where $Ro$ is the Rossby number $Ro = U/(fR)$, $N$ is the Brunt-Väisälä frequency, $D_h = fL/N$ is the depth scale, $R_L = U/(fL)$ is another Rossby number. The full derivation of this scaling by *Allen and Hickey* [2010] can be found in the appendix.

### 2.2.4 Scaling of the Upwelling Flux

The upwelling flux is the flux of water upwelled onto the shelf. The scaling for the flux of water upwelled onto the shelf was accomplished by estimating the speed and vertical thickness of the upwelling stream [*Allen and Hickey*, 2010]. The scaling for the upwelling flux is as follows:

$$\Phi = U_* W_{sb} Z = (UW_{sb}D_h)F^{3/2}R_L^{1/2} \tag{2}$$

where $\Phi$ is the upwelling flux, $U_*$ is the velocity of the upwelling stream, and $W_{sb}$ is the width of the canyon at the shelf break. The full derivation of this scaling by *Allen and Hickey* [2010] can also be found in the appendix.

# 3 Methodology

## 3.1 The Model

Using the Massachusetts Institute of Technology general circulation model (MITgcm) [*Marshall et al.*, 1997] numerous experiments of upwelling over canyons in a laboratory tank were simulated. This model was created to model the ocean, atmosphere and climate. It uses the Navier Stokes Equations and has the capability of being non-hydrostatic. The model can be used on both large and small scales and can be applied to this laboratory experiment.

## 3.2 The Experiment Setup

The scenario modeled consists of a canyon in a laboratory tank as per *Dawe and Allen* [2010]. There is a canyon cutting into the continental shelf with the center consisting of a flat abyss (Figure 4). A central cylinder was added to the topography to maintain numerical stability [*Dawe and Allen*, 2010].

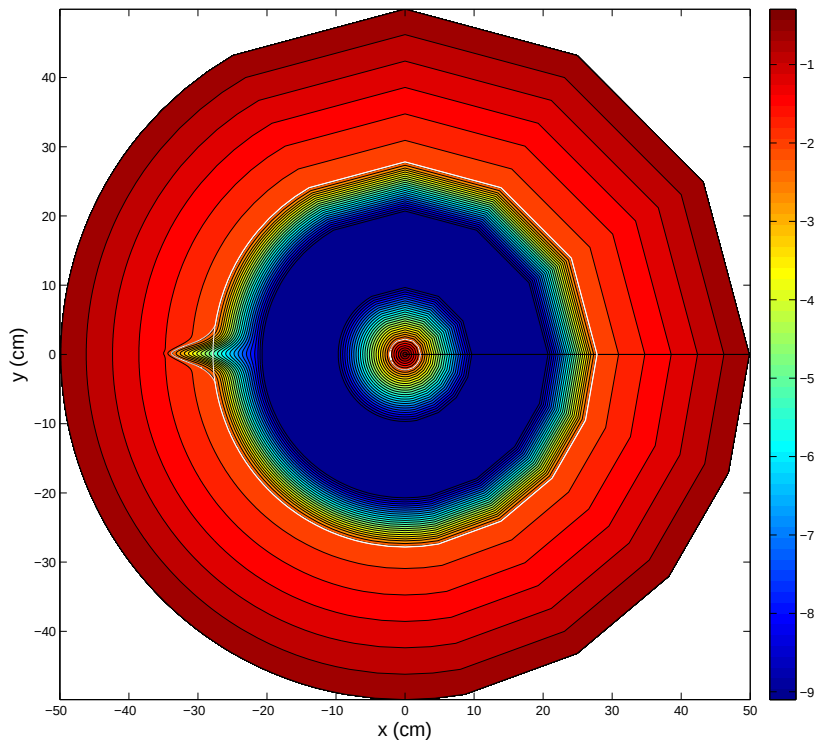


Figure 4: A contour plot of the Basic slope topography in a tank. The topography contours are in centimeters. The white contours show the 2 cm shelf break depth and in the center is the cylinder.

The model was run using cylindrical coordinates. The model used a viscosity of $10^{-6}$ m$^2$s$^{-1}$ and a diffusion coefficient of $1.5\times10^{-9}$ m$^2$s$^{-1}$, both are molecular values for water. The model was run assuming that the system was non-hydrostatic to allow for internal waves, but the results were very similar to the hydrostatic case [*Dawe and Allen*, 2010]. Other specified values included a forcing velocity of 0.3 ms$^{-1}$ which is flowing clockwise in the tank and the topography of the tank.

The different cases included in the experiment consisted of varying the stratification in the tank by changing the Brunt-Väisälä frequency, $N$; the rotation rate of the tank

by varying the Coriolis parameter, $f$; and by varying the slope of the continental shelf (Figure 5). A table consisting of the varied parameters are included in Table 1 and Table 2 includes the values of these parameters for the different cases along with the radius of curvature, $R$, and the canyon width, $W$, both of which are used for different calculations for the Rossby number, $Ro$; and the upstream velocity $U$.

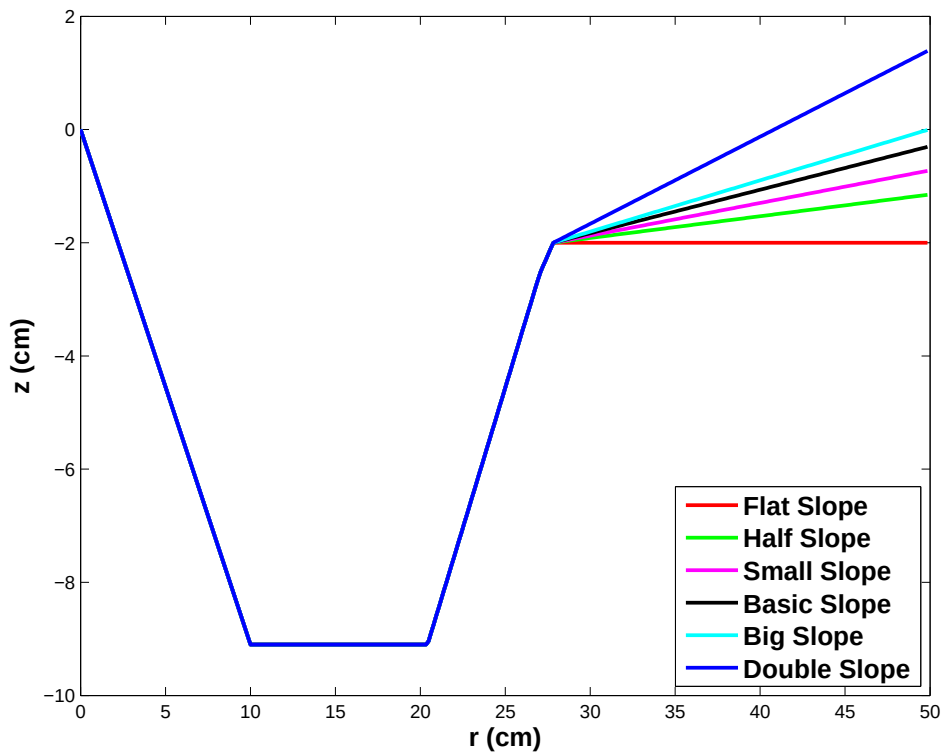


Figure 5: Cross sections of the topography from the center to the wall of the tank as shown in Figure 4. These cross sections are taken away from the canyon and illustrates the different slopes used in the various canyon cases.

Table 1: Shows the values of the parameters varied.

| Parameter | Basic | High Value | Low Value |
|---|---|---|---|
| $N$ ($s^{-1}$) | 2.2 | 4.4 | 1.1 |
| $f$ ($s^{-1}$) | 0.52 | 0.62 | 0.42 |
| Slope | Basic | Double | Flat |

| Slope Range | | | | | |
|---|---|---|---|---|---|
| Flat | Half | Small | Basic | Big | Double |
| 0.000 | 0.039 | 0.058 | 0.077 | 0.09 | 0.15 |

Table 2: Values for the different cases with corresponding error. $f$ is the Coriolis parameter, $N$ is the Brunt-Väisälä frequency, $s$ is the shelf slope, $R$ is the radius of curvature of the canyon, $W$ is the width of the canyon, $U$ is the velocity upstream of the canyon, and $Ro$ are Rossby numbers. Determination of the error will be explained later.

| Case | $f$ (s$^{-1}$) | $N$(s$^{-1}$) | $s$ | $R$ (cm) | $W(cm)$ | $U$ | $Ro = U/fR$ | $Ro = U/fW$ |
|---|---|---|---|---|---|---|---|---|
| Basic | 0.52 | 2.2 | 0.077 ± 0.008 | 3.8 ± 0.2 | 2.69 ± 0.03 | 1.35 ± 0.02 | 0.69 ± 0.04 | 0.97 ± 0.02 |
| Basic Low N | 0.52 | 1.1 | 0.077 ± 0.008 | 3.8 ± 0.2 | 2.69 ± 0.03 | 1.29 ± 0.02 | 0.66 ± 0.04 | 0.92 ± 0.02 |
| Basic High N | 0.52 | 4.4 | 0.077 ± 0.008 | 3.8 ± 0.2 | 2.69 ± 0.03 | 1.43 ± 0.02 | 0.73 ± 0.04 | 1.02 ± 0.02 |
| Basic Low f | 0.42 | 2.2 | 0.077 ± 0.008 | 3.8 ± 0.2 | 2.69 ± 0.03 | 1.40 ± 0.02 | 0.88 ± 0.05 | 1.24 ± 0.02 |
| Basic High f | 0.62 | 2.2 | 0.077 ± 0.008 | 3.8 ± 0.2 | 2.69 ± 0.03 | 1.30 ± 0.02 | 0.55 ± 0.03 | 0.78 ± 0.01 |
| Double Slope | 0.52 | 2.2 | 0.15 ± 0.02 | 3.8 ± 0.2 | 1.970 ± 0.009 | 1.31 ± 0.02 | 0.67 ± 0.04 | 1.28 ± 0.02 |
| Double Slope Low N | 0.52 | 1.1 | 0.15 ± 0.02 | 3.8 ± 0.2 | 1.970 ± 0.009 | 1.30 ± 0.02 | 0.66 ± 0.04 | 1.27 ± 0.02 |
| Double Slope High N | 0.52 | 4.4 | 0.15 ± 0.02 | 3.8 ± 0.2 | 1.970 ± 0.009 | 1.33 ± 0.02 | 0.68 ± 0.04 | 1.30 ± 0.02 |
| Double Slope Low f | 0.42 | 2.2 | 0.15 ± 0.02 | 3.8 ± 0.2 | 1.970 ± 0.009 | 1.34 ± 0.02 | 0.84 ± 0.05 | 1.62 ± 0.03 |
| Double Slope High f | 0.62 | 2.2 | 0.15 ± 0.02 | 3.8 ± 0.2 | 1.970 ± 0.009 | 1.27 ± 0.02 | 0.54 ± 0.03 | 1.04 ± 0.02 |
| Half Slope | 0.52 | 2.2 | 0.039 ± 0.004 | 4.0 ± 0.2 | 3.18 ± 0.02 | 1.26 ± 0.02 | 0.61 ± 0.03 | 0.76 ± 0.01 |
| Half Slope Low N | 0.52 | 1.1 | 0.039 ± 0.004 | 4.0 ± 0.2 | 3.18 ± 0.02 | 1.15 ± 0.02 | 0.56 ± 0.03 | 0.70 ± 0.01 |
| Half Slope High N | 0.52 | 4.4 | 0.039 ± 0.004 | 4.0 ± 0.2 | 3.18 ± 0.02 | 1.35 ± 0.02 | 0.66 ± 0.03 | 0.82 ± 0.01 |
| Half Slope Low f | 0.42 | 2.2 | 0.039 ± 0.004 | 4.0 ± 0.2 | 3.18 ± 0.02 | 1.33 ± 0.02 | 0.78 ± 0.04 | 1.00 ± 0.02 |
| Half Slope High f | 0.62 | 2.2 | 0.039 ± 0.004 | 4.0 ± 0.2 | 3.18 ± 0.02 | 1.21 ± 0.02 | 0.50 ± 0.03 | 0.61 ± 0.01 |
| Flat Slope | 0.52 | 2.2 | 0.000 ± 0.002 | 2.9 ± 0.2 | 2.97 ± 0.04 | 1.20 ± 0.02 | 0.79 ± 0.06 | 0.78 ± 0.02 |
| Flat Slope Low N | 0.52 | 1.1 | 0.000 ± 0.002 | 2.9 ± 0.2 | 2.97 ± 0.04 | 1.09 ± 0.02 | 0.72 ± 0.05 | 0.71 ± 0.02 |
| Flat Slope High N | 0.52 | 4.4 | 0.000 ± 0.002 | 2.9 ± 0.2 | 2.97 ± 0.04 | 1.27 ± 0.02 | 0.84 ± 0.06 | 0.82 ± 0.02 |
| Flat Slope Low f | 0.42 | 2.2 | 0.000 ± 0.002 | 2.9 ± 0.2 | 2.97 ± 0.04 | 1.28 ± 0.02 | 1.04 ± 0.07 | 1.03 ± 0.02 |
| Flat Slope High f | 0.62 | 2.2 | 0.000 ± 0.002 | 2.9 ± 0.2 | 2.97 ± 0.04 | 1.13 ± 0.02 | 0.62 ± 0.04 | 0.61 ± 0.01 |
| Big Slope | 0.52 | 2.2 | 0.09 ± 0.01 | 2.9 ± 0.2 | 1.76 ± 0.01 | 1.35 ± 0.02 | 0.90 ± 0.06 | 1.48 ± 0.02 |
| Big Slope Low N | 0.52 | 1.1 | 0.09 ± 0.01 | 2.9 ± 0.2 | 1.76 ± 0.01 | 1.31 ± 0.02 | 0.87 ± 0.06 | 1.43 ± 0.02 |
| Big Slope High N | 0.52 | 4.4 | 0.09 ± 0.01 | 2.9 ± 0.2 | 1.76 ± 0.01 | 1.43 ± 0.02 | 0.95 ± 0.07 | 1.56 ± 0.03 |
| Big Slope Low f | 0.42 | 2.2 | 0.09 ± 0.01 | 2.9 ± 0.2 | 1.76 ± 0.01 | 1.41 ± 0.02 | 1.16 ± 0.08 | 1.91 ± 0.03 |
| Big Slope High f | 0.62 | 2.2 | 0.09 ± 0.01 | 2.9 ± 0.2 | 1.76 ± 0.01 | 1.31 ± 0.02 | 0.73 ± 0.05 | 1.20 ± 0.02 |
| Small Slope | 0.52 | 2.2 | 0.058 ± 0.006 | 3.0 ± 0.2 | 1.99 ± 0.01 | 1.31 ± 0.02 | 0.85 ± 0.06 | 1.27 ± 0.02 |
| Small Slope Low N | 0.52 | 1.1 | 0.058 ± 0.006 | 3.0 ± 0.2 | 1.99 ± 0.01 | 1.23 ± 0.02 | 0.80 ± 0.06 | 1.19 ± 0.02 |
| Small Slope High N | 0.52 | 4.4 | 0.058 ± 0.006 | 3.0 ± 0.2 | 1.99 ± 0.01 | 1.41 ± 0.02 | 0.92 ± 0.06 | 1.36 ± 0.02 |
| Small Slope Low f | 0.42 | 2.2 | 0.058 ± 0.006 | 3.0 ± 0.2 | 1.99 ± 0.01 | 1.37 ± 0.02 | 1.11 ± 0.08 | 1.64 ± 0.03 |
| Small Slope High f | 0.62 | 2.2 | 0.058 ± 0.006 | 3.0 ± 0.2 | 1.99 ± 0.01 | 1.26 ± 0.02 | 0.69 ± 0.05 | 1.02 ± 0.02 |

### 3.3 Incorporating Shelf Slope in the Scaling

As mentioned earlier the initial scaling did not include a variation of the shelf slope, but after investigation it appears to have an effect on the upwelling. To account for the shelf slope in the scaling of the depth of upwelling and the flux of water upwelled onto the shelf a non-dimensional number will be introduced. The origin of this number will be determined by re-evaluating the derivation of the original scaling and trying to incorporate the shelf slope. It is likely that the non-dimensional number will be a function of the slope of the shelf, and other vertical and horizontal parameters such as the buoyancy frequency and Coriolis parameter, respectively.

To test the scaling plots of observations from the MITgcm model versus scaled values for the depth of upwelling and upwelling flux will be made. The more linear the plot and less scatter means that the scaled quantities are close to the observations. The norm of residuals will be used to measure goodness of fit of the scaled values to the observations. Error bars will be included to set a range of acceptable values; the method for determining error will be discussed later.

## 4 Initial Results

### 4.1 Scaling

Simulations of upwelling events over submarine canyons in a one meter diameter tank were run using the MITgcm model. These simulations varied the shelf slope along with the stratification and Coriolis parameter. Calculations for the depth of upwelling and the upwelling flux are made from the output data. The depth of upwelling is defined as the difference between the deepest water that arrives on the shelf at head depth and the head depth of the canyon. The upwelling flux is defined as the volume of water that comes up through the canyon during the last period of upwelling, in this case, over the last five seconds of the run time. Then using the canyon geometry and the velocity over the canyon scales for the upwelling depth and flux were found using the scales derived by *Allen and Hickey* [2010]. The observed and scaled values of the upwelling depth and flux are included in Figure 6. These plots are not as linear as those in Figure 1 and also have a larger norm of residuals indicating much scatter from the line of best fit.

Figure 6a shows that in general the normalized measured upwelling depth is greatest for the low Coriolis parameter cases followed by low stratification cases, cases with only

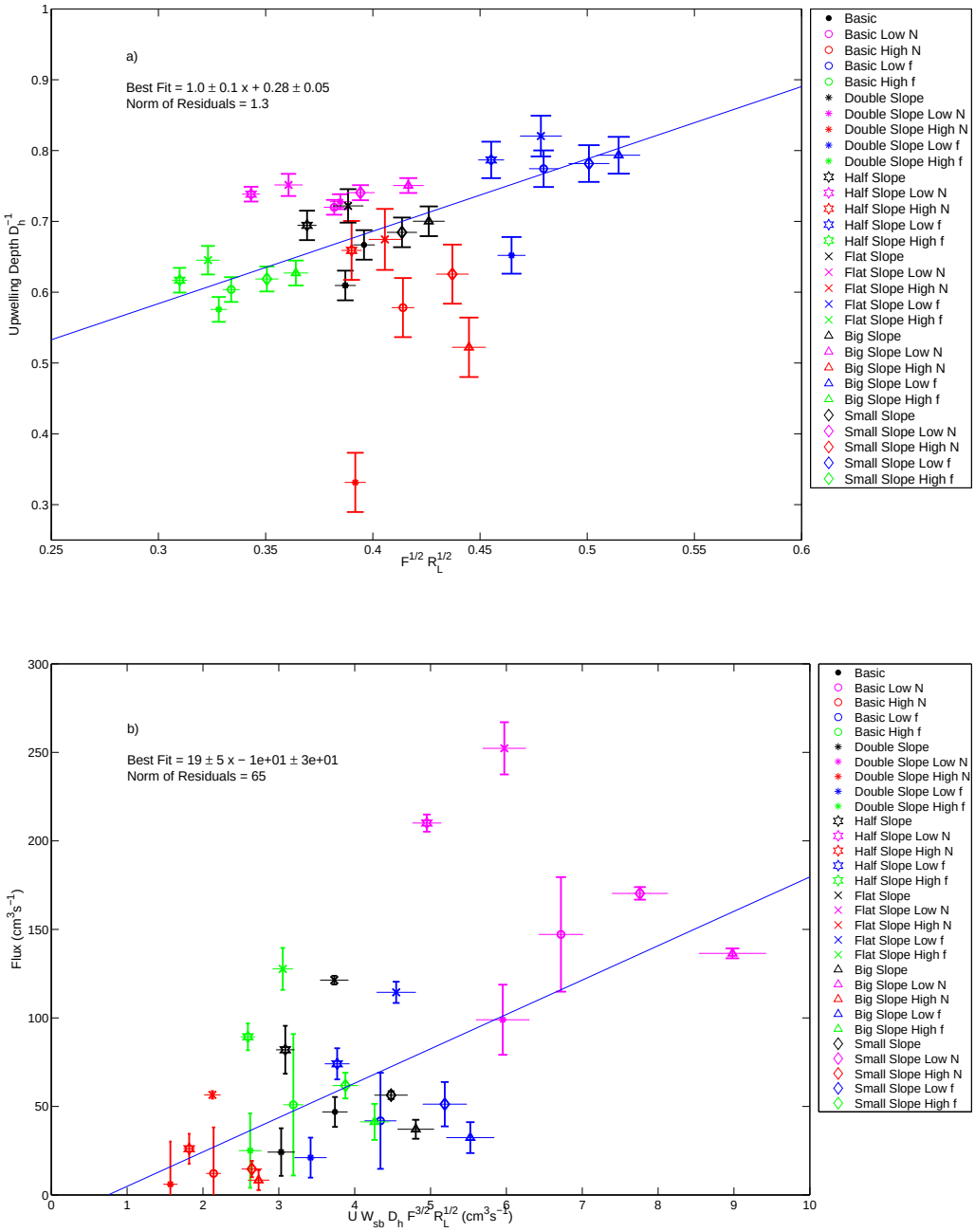


Figure 6: Observed versus scaled plots for a) the depth of upwelling and b) the upwelling flux using the original scales from *Allen and Hickey* [2010]. The line of best fit was found using all points but those corresponding to the double or flat slope cases because those slopes were extreme; and in a) the high or low $N$ cases were also unused because they were outliers. The norm of residuals is normalized to the x-axis.

variation in slope, high Coriolis parameter cases, and with the high stratification cases having the shallowest normalized upwelling depth. Within each of these groupings the cases with smaller slopes tend to have the deepest upwelling depths and steeper slope cases tend to have lower upwelling depths. The low stratification cases have very little variation even with different shelf slopes. The measured depth of upwelling for the high stratification cases have much variation compared to the basic and low stratification, or Coriolis parameter variation cases. The variations in the Coriolis parameter cases follow the line of best fit better than the stratification cases.

Figure 6b shows that in general the measured flux is largest for low stratification cases, lowest for high stratification cases and everything else lies in between. Within each stratification or Coriolis parameter grouping the flatter slope cases have the largest flux and the cases with steeper slopes have the smaller fluxes. Looking at the plot it can be seen that there is much scatter about the line of best fit which is also indicated by a large norm of residuals.

## 4.2 Time Series

### 4.2.1 Depth of Upwelling

Time series for the depth of upwelling were created to better understand what is happening during the upwelling event (Figure 7). The high stratification cases have the lowest depth of upwelling and the low stratification cases have the deepest depth of upwelling over the full 30 s. The other cases have less variation, but the low Coriolis parameter has a slightly smaller upwelling depth than the high Coriolis parameter case over the full 30 s.

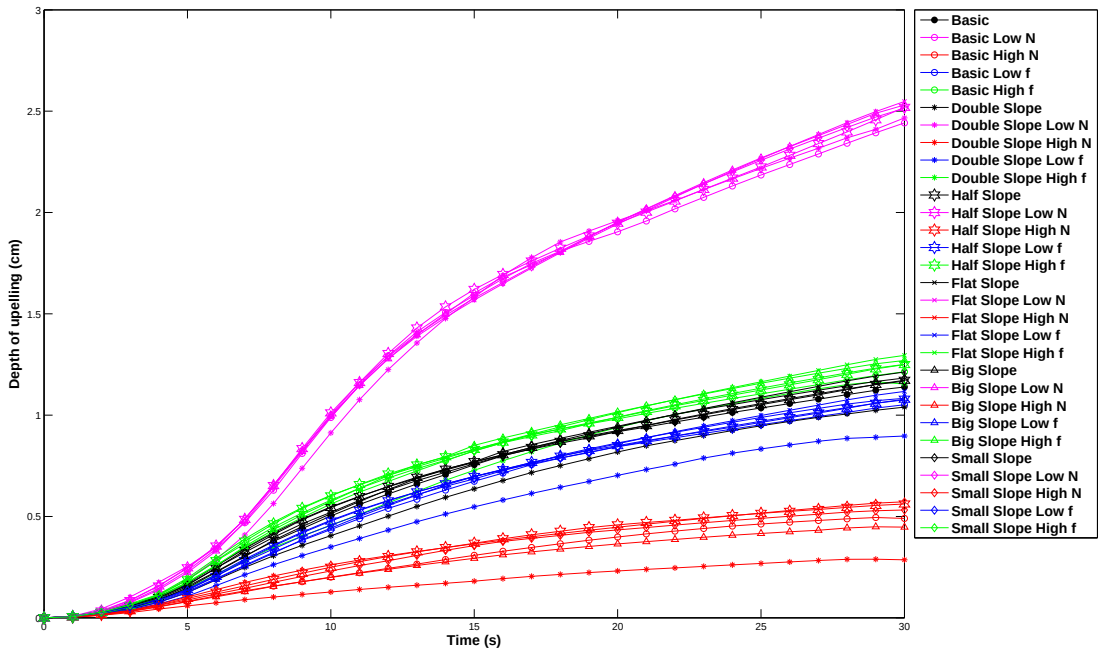


Figure 7: Time series for the upwelling depth for the whole duration of the upwelling event.

The variation between the different slopes for the low stratification cases is much smaller than the variation between the different slopes for the high stratification case. For the low stratification cases the flat slope had the deepest upwelling depth followed by the big slope, half slope, small slope, double slope, and with the basic slope having the shallowest upwelling depth at 30 s. For the high stratification cases the flatter slope cases had the deepest upwelling depths and steeper slope cases have shallower upwelling depths at 30 s.

### 4.2.2 Volume of Water Upwelled

Time series for the volume of water onto the shelf were created to better understand what is happening during the upwelling event (Figure 8). The high stratification cases have the smallest volume of water upwelled onto the shelf after 25 s and the low stratification cases have the largest amount of water upwelled onto the shelf after 10 s. Before these times the volume is very close and nearly indistinguishable between the other cases. The variations in the Coriolis parameter and the cases in which only the slope was varied cover about the same range of upwelled water volume at all times.

The slope of the lines for the low stratification cases is much greater than the slope of the line for the high stratification cases. The slope of these lines between 25 s and 30 s gives the upwelling flux.

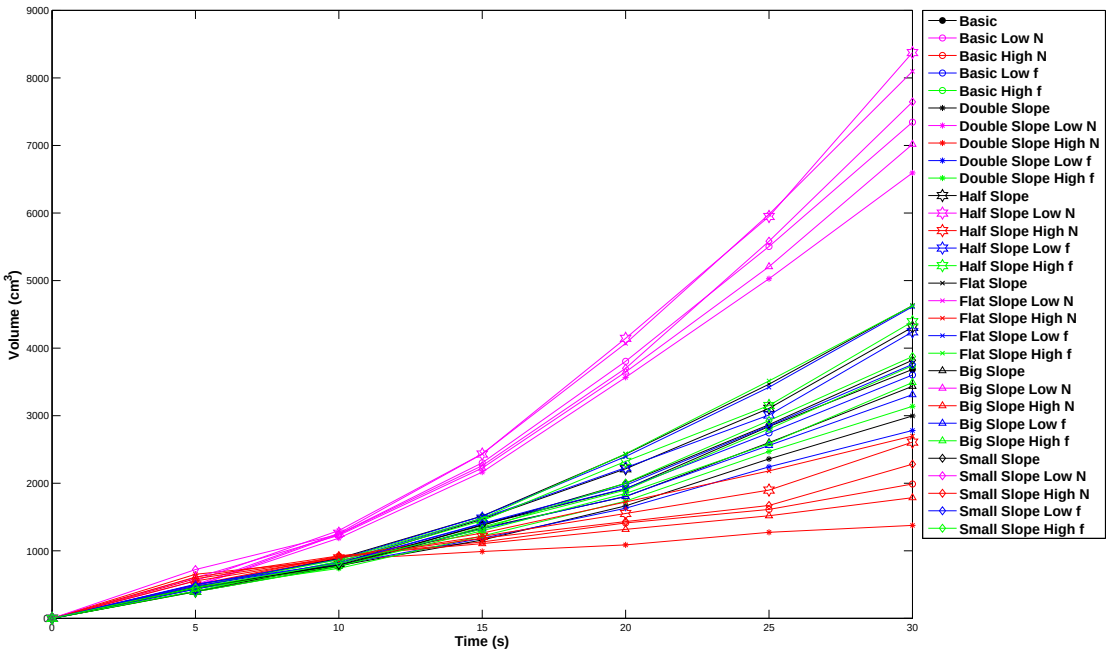


Figure 8: Time series for the volume of water upwelled onto the shelf for the whole duration of the upwelling event.

# 5 Inclusion of Shelf Slope in the Scaling

## 5.1 Slope Effect on the Pressure Field

As mentioned earlier submarine canyons enhance the upwelling onto the shelf. As a larger volume of denser water arrives on the shelf this has the potential to create a back pressure making further upwelling more difficult. If the slope of the shelf were flat then the water upwelled would likely continue to flow up the shelf or be carried away. If the shelf slope were to have a steep slope then the head of the canyon would be at a shallower depth and thus shallower water would make it onto the shelf, but since the definition of the upwelling depth is the difference of the depth of the deepest water which reached the head and the head depth there is another factor which will cause this difference to

shorten.

The isopycnals which reach the shelf will follow the slope of the shelf. If the slope is not flat then the water that get upwelled will have a more difficult time moving up the shelf because there is dense water already there. This denser water will create a back pressure and restrict the movement of water up the shelf.

To find the baroclinic pressure gradient force at the upwelling depth, $Z$, use the hydrostatic pressure gradient:

$$\frac{\partial p}{\partial z} = -\rho g \tag{3}$$

where $p$ is pressure, $\rho$ is the density, and $g$ is the gravitational acceleration.

Rearranging (3) to find the change in pressure at the upwelling depth between the mouth and head of the canyon and adding the effect of the slope to the pressure:

$$\Delta p = -\Delta\rho g Z \beta(s, N, f) \tag{4}$$

where $\Delta p$ is the pressure difference along depth $Z + H_h$ where $Z$ is the upwelling depth and $H_h$ is the head depth; $\Delta\rho$ is the density difference along depth $Z + H_h$ and given by $\Delta\rho = \partial\rho_*/\partial z Z\beta(s, N, f)$, where $\rho_*$ is the undisturbed horizontal density; and $g$ is the gravitational acceleration. The function $\beta$ adds some back pressure due to the slope, where $N$ is the Brunt-Väisälä frequency, $s$ is the shelf slope, and $f$ is the Coriolis parameter.

The function $\beta$ in equation 4 acts to add some back pressure due to the slope and restrict the water from moving further up the shelf. It should be a function of the slope, $s$, because a greater slope should create a greater back pressure due to gravity acting on the dense water on the shelf; also a function of $N$ because there is a stronger density gradient and with more dense water on the shelf creates more back pressure; and a function of $f^{-1}$ because the bottom Ekman layer is defined by:

$$\delta = \frac{\sqrt{2\nu}}{f} \tag{5}$$

where $\delta$ is the thickness of the Ekman layer and $\nu$ is the viscosity. Thus upwelled water on the shelf with a lower $f$ will have a thicker layer and creates more back pressure.

Figure 9 shows how water movement is restricted for steeper slopes and low $f$. The isohalines (which are taken to reflect the density) follow the slope of the shelf, so if the shelf slope were flat there should be no back pressure and if the shelf slope were steep

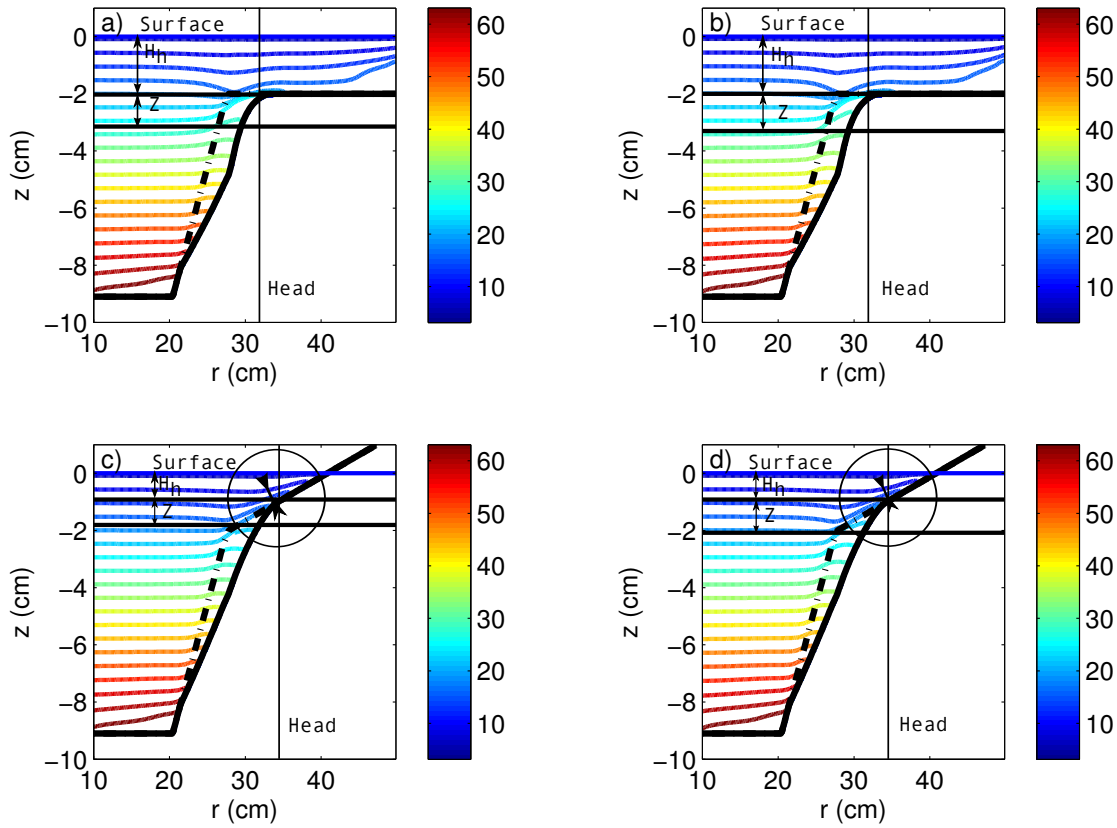


Figure 9: Isohalines over a) a flat slope canyon under low $f$ conditions, b) a flat slope canyon under high $f$ conditions, c) a double slope canyon under low $f$ conditions, and d) a double slope canyon under high $f$ conditions. The head depth, $H_h$; upwelling depth, $Z$; and head of the canyon are shown. The circled regions highlight the thickness of the upwelled water on the shelf.

then flow up the shelf will have the weight of the water further up the shelf acting against it and creating a larger pressure. For lower $f$ the width of the upwelled water for a given isohaline is thicker compared to a higher $f$ which is shown in the circles by an arrow between the topography and an isohaline. A thicker water mass that reaches the same horizontal extent from the head will have a larger mass and a greater weight associated with it, so this will create more back pressure.

If $s$, $N$, and $f^{-1}$ are all included then all components of the topographic Burger number will be present. The topographic Burger number, $sN/f$, is found in many examples of flow along slopes [*Brink and Lentz*, 2010; *Lentz and Chapman*, 2004; *Jacox and Edwards*, 2011]. The topographic Burger number measures the importance of the bottom slope

and so a large Burger number means that the buoyancy transport effects are important to the problem [*Brink and Lentz*, 2010].

Another explanation for the origin of the Burger number, and back pressure in this case, can be related to a study by *Nof* [1982]. As the flow comes out of the page in Figure 10 there is a gravitational force acting to pull the water down the slope which is balanced by the Coriolis force pulling the water further up slope [*Nof*, 1982]. Writing this balance as:

$$g's = fu \tag{6}$$

Where $g'$ is the reduced gravity defined by $g' = (\Delta\rho/\rho)g$, and $u$ is the along-isobath velocity. Rearranging for $u$:

$$u = \frac{g's}{f} \tag{7}$$

Since $N = (-g/\rho_o)\partial\rho_*/\partial z$ and is a function of $g$ there is a relation to the velocity of the flow and the topographic Burger number.

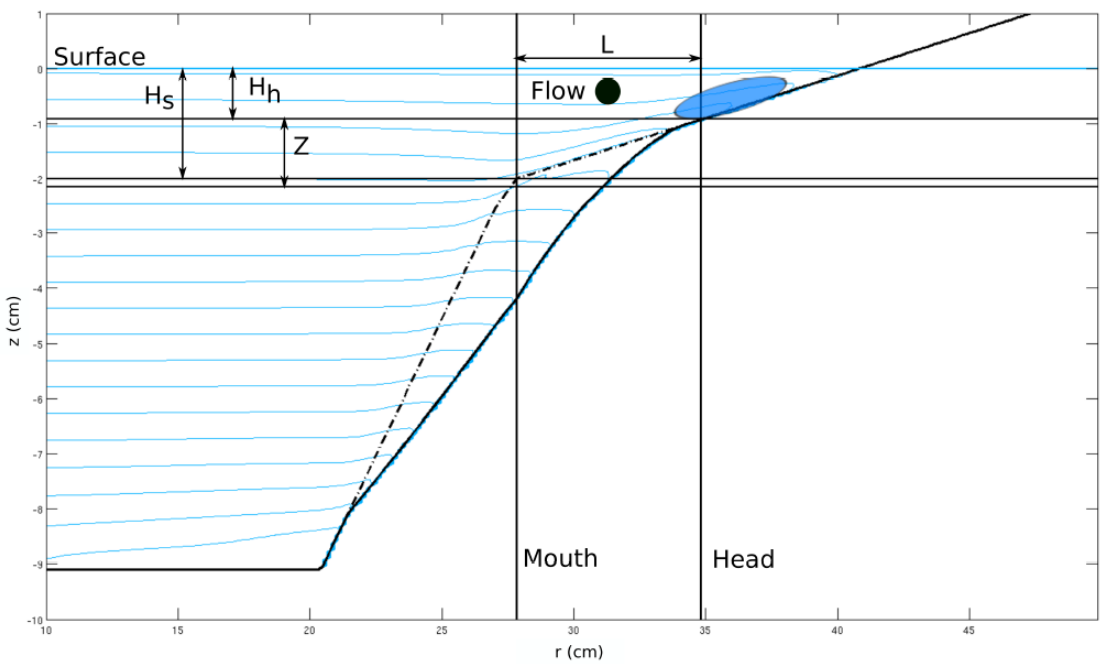


Figure 10: A cross section of a double slope canyon with tilted isohalines. The key depth parameters are also shown: the head depth, $H_h$; the shelf break depth, $H_s$; and the depth of upwelling, $Z$ (it should be noted that the $Z$ was drawn a bit deeper to make it more visibly distinct from $H_s$). The length of the canyon, $L$, is also shown. The flow is coming out of the page as indicated by the •. The gravitational force acting down the slope is balanced by the Coriolis force acting up slope.

Here the gravitational force is also balanced by the Coriolis force which should have the $u$ velocity to the left, but in this case the flow is to the right of the Coriolis force. The dense water on the shelf will want to flow the other way keeping the shallower water to the right of the flow [*Nof*, 1982]. This could result in the potential for the water to move down slope, back towards the canyon, and thus is a potential source of the back pressure due to the water mass on the shelf.

Now that the parameters significant to creating the added back pressure characterized by $\beta$ has been established the change in pressure at $Z + H_h$ becomes:

$$\Delta p = -g\frac{\partial \rho_*}{\partial z} Z^2 \beta(s, N, f) \tag{8}$$

This is the change in pressure between the mouth and the head of the canyon.

## 5.2 Scaling for the Depth of Upwelling

To determine the scale for the depth of upwelling, $Z$, follow the same steps by *Allen and Hickey* [2010] which are found in the appendix.

The Baroclinic pressure gradient force is found by dividing (8) by $L$. Equating this to the Barotropic pressure gradient force above the canyon which is defined as $\rho_o f U F$ [*Allen and Hickey*, 2010]. Now rearranging the same way as *Allen and Hickey* [2010] the depth of upwelling scale becomes:

$$Z = \beta(s, N, f)^{-1/2} D_h (F R_L)^{1/2} \tag{9}$$

where $Z$ is the upwelling depth, $f$ is the Coriolis parameter, $U$ is the velocity upstream of the canyon, $L$ is the length of the canyon, $F$ is a function used to relate velocities $U$ and $V$ as flow crosses the canyon, $N$ is the Brunt-Väisälä frequency, $D_h = fL/N$ is the depth scale, $R_L = U/(fL)$ is a Rossby number, and $\beta$ is a non-dimensional number which accounts for the shelf slope.

From experimentation with data from the MITgcm model to fit a linear line for the observed and scaled values of the depth of upwelling it can be found that:

$$\beta^{-1} = \exp\left(\frac{asN}{f}\right) \tag{10}$$

where $a$ is a coefficient which has included the 1/2 exponent and determines the steepness of the exponential, $s$ is the slope of the shelf, $N$ is the Brunt-Väisälä frequency, and $f$

is the Coriolis parameter. Verification of this number will be shown later using the data from the MITgcm model.

Thus, the depth of upwelling scale can be expressed as:

$$Z = \exp\left(\frac{a_1 sN}{f}\right) D_h (FR_L)^{1/2} \tag{11}$$

### 5.3 Scaling for the Upwelling Flux

Using the same methodology as *Allen and Hickey* [2010] as outlined in the appendix, the scaling for the upwelling flux can be expressed as:

$$\Phi = \exp\left(\frac{a_2 sN}{f}\right) (UW_{sb} D_h) F^{3/2} R_L^{1/2} \tag{12}$$

where $\Phi$ is the upwelling flux, $U_*$ is the velocity of the upwelling stream, and $W_{sb}$ is the width of the canyon at the shelf break.

Note that the coefficients $a_1$ and $a_2$ in the depth of upwelling and upwelling flux are different. Their determination will be explained in the next section.

## 6 Determination and Verification of $\beta$

### 6.1 Early Attempts

As shown above in Figures 1 and 6, the shelf slope clearly affects both the depth of upwelling and the amount of water that upwells onto the shelf. Steeper slopes have a shallower upwelling depth and a smaller flux. These plots also do not have a very linear relation between the observed and the scaled values as there is much scatter about the line of best fit. To improve the scaling and create a more linear plot with less scatter, a non-dimensional number will be determined and incorporated into the original scaling from *Allen and Hickey* [2010].

To start examining the influence of the shelf slope in the upwelling depth and the upwelling flux a hypothesis was made that the role of the shelf slope would have to do with the shelf slope, the buoyancy frequency and the Coriolis parameter. To test this hypothesis variations of the above were included into the original scaling and plotted against the measured values. The more linear the plot and the smaller the norm of residuals the better the scaling is at representing the modelled results.

The most linear plot was given by the flux with the non-dimensional number representing the slope as $f/(sN)$ where s is the shelf slope (Figure 11a). However, did not work with the depth of upwelling(Figure 11b). Also because there was a division by the shelf slope the flat slope cases went to infinity.

## 6.2 Later Results

To correct for the flat slope cases going to infinity, an exponential was used, making the new non-dimensional number $\beta^{-1} = \exp(aNs/f)$ (Figures 12 and 13). The values for these non-dimensional numbers can be found in Table 3.

Previous work has used the Rossby number as a function of the radius of curvature [*Allen and Hickey*, 2010], but here both a Rossby number as a function of the radius of curvature, $R$ and as a function of the canyon width, $W$ are used to see which scales better. The significance of this is whether $W$ or $R$ determines if the flow will follow the isobaths or cross the canyon and drive upwelling [*Allen and Hickey*, 2010].

These figures (12 and 13) have a coefficient $a_1$ for the depth of upwelling and $a_2$ for the upwelling flux, which is determined by finding the slope of the weighted least-squares fit to the linearized plots found in Figures 14 and 15 where those points with the smallest error associated with them have the highest weighting, and in some cases masking out a highly weighted outlier. Values for these coefficients are found in Table 4.

## 6.3 Error Analysis

Error bars are added to the plots to get a better understanding of how well the scaling fits the observations. If the line of best fit goes through the error bars of most of points then the scaling is successful.

The error bars are found by using standard fractional error techniques [e.g. *Bevington*, 1969].

### 6.3.1 Error in the Depth of Upwelling

The fractional error in the y-axis on the depth of upwelling plots in Figures 1a, 6a, and 12 is:

$$\frac{\sigma_y}{y} = \sqrt{\frac{\sigma_Z^2}{Z^2} + \frac{\sigma_{D_h}^2}{D_h^2}} \tag{13}$$

Table 3: These are the values for the non-dimensional number used in the scaling with corresponding error.

| Case | $sN/f$ | $\beta^{-1}Z(R)$ | $\beta^{-1}Z(W)$ | $\beta^{-1}flux(R)$ | $\beta^{-1}flux(W)$ |
|---|---|---|---|---|---|
| Basic | 0.33 ± 0.04 | 0.85 ± 0.02 | 1.24 ± 0.04 | 0.42 ± 0.05 | 0.36 ± 0.05 |
| Basic Low N | 0.16 ± 0.02 | 0.92 ± 0.01 | 1.11 ± 0.02 | 0.65 ± 0.04 | 0.60 ± 0.04 |
| Basic High N | 0.65 ± 0.07 | 0.72 ± 0.04 | 1.54 ± 0.09 | 0.17 ± 0.04 | 0.13 ± 0.03 |
| Basic Low f | 0.40 ± 0.04 | 0.82 ± 0.03 | 1.31 ± 0.05 | 0.34 ± 0.05 | 0.28 ± 0.05 |
| Basic High f | 0.27 ± 0.03 | 0.87 ± 0.02 | 1.20 ± 0.03 | 0.48 ± 0.05 | 0.42 ± 0.05 |
| Double Slope | 0.65 ± 0.07 | 0.72 ± 0.04 | 1.54 ± 0.09 | 0.17 ± 0.04 | 0.13 ± 0.03 |
| Double Slope Low N | 0.33 ± 0.03 | 0.85 ± 0.02 | 1.24 ± 0.04 | 0.42 ± 0.05 | 0.36 ± 0.05 |
| Double Slope High N | 1.3 ± 0.1 | 0.52 ± 0.06 | 2.4 ± 0.3 | 0.03 ± 0.01 | 0.016 ± 0.008 |
| Double Slope Low f | 0.81 ± 0.09 | 0.67 ± 0.05 | 1.7 ± 0.1 | 0.12 ± 0.03 | 0.078 ± 0.03 |
| Double Slope High f | 0.55 ± 0.06 | 0.76 ± 0.04 | 1.43 ± 0.07 | 0.23 ± 0.05 | 0.18 ± 0.04 |
| Half Slope | 0.16 ± 0.02 | 0.92 ± 0.01 | 1.11 ± 0.02 | 0.65 ± 0.04 | 0.60 ± 0.04 |
| Half Slope Low N | 0.081 ± 0.009 | 0.960 ± 0.007 | 1.06 ± 0.008 | 0.80 ± 0.02 | 0.77 ± 0.03 |
| Half Slope High N | 0.33 ± 0.04 | 0.85 ± 0.02 | 1.24 ± 0.04 | 0.42 ± 0.05 | 0.35 ± 0.05 |
| Half Slope Low f | 0.20 ± 0.02 | 0.90 ± 0.02 | 1.14 ± 0.02 | 0.58 ± 0.04 | 0.53 ± 0.05 |
| Half Slope High f | 0.14 ± 0.02 | 0.93 ± 0.01 | 1.09 ± 0.01 | 0.69 ± 0.04 | 0.65 ± 0.04 |
| Flat Slope | 0.000± 0.007 | 1.000 ± 0.003 | 1.000 ± 0.004 | 1.00 ± 0.02 | 1.00 ± 0.02 |
| Flat Slope Low N | 0.000 ± 0.003 | 1.000 ± 0.002 | 1.000 ± 0.002 | 1.000 ± 0.009 | 1.00 ± 0.01 |
| Flat Slope High N | 0.00 ± 0.01 | 1.000 ± 0.007 | 1.000 ± 0.009 | 1.00 ± 0.04 | 1.00 ± 0.04 |
| Flat Slope Low f | 0.000 ± 0.008 | 1.000 ± 0.004 | 1.000 ± 0.006 | 1.00 ± 0.02 | 1.00 ± 0.03 |
| Flat Slope High f | 0.000 ± 0.006 | 1.000 ± 0.003 | 1.000 ± 0.004 | 1.00 ± 0.02 | 1.00 ± 0.02 |
| Big Slope | 0.38 ± 0.04 | 0.82 ± 0.03 | 1.29 ± 0.04 | 0.36 ± 0.05 | 0.30 ± 0.05 |
| Big Slope Low N | 0.19 ± 0.02 | 0.91 ± 0.01 | 1.13 ± 0.02 | 0.60 ± 0.04 | 0.54 ± 0.04 |
| Big Slope High N | 0.77 ± 0.08 | 0.68 ± 0.04 | 1.7 ± 0.1 | 0.13 ± 0.04 | 0.09 ± 0.03 |
| Big Slope Low f | 0.47 ± 0.05 | 0.79 ± 0.03 | 1.37 ± 0.06 | 0.28 ± 0.05 | 0.22 ± 0.04 |
| Big Slope High f | 0.32 ± 0.03 | 0.85 ± 0.02 | 1.24 ± 0.04 | 0.42 ± 0.05 | 0.36 ± 0.05 |
| Small Slope | 0.24 ± 0.03 | 0.88 ± 0.02 | 1.18 ± 0.03 | 0.52 ± 0.05 | 0.46 ± 0.05 |
| Small Slope Low N | 0.12 ± 0.01 | 0.94 ± 0.01 | 1.08 ± 0.01 | 0.72 ± 0.03 | 0.68 ± 0.03 |
| Small Slope High N | 0.49 ± 0.05 | 0.78 ± 0.03 | 1.38 ± 0.06 | 0.27 ± 0.05 | 0.21 ± 0.04 |
| Small Slope Low f | 0.30 ± 0.03 | 0.86 ± 0.02 | 1.22 ± 0.03 | 0.44 ± 0.05 | 0.38 ± 0.05 |
| Small Slope High f | 0.20 ± 0.02 | 0.90 ± 0.02 | 1.14 ± 0.02 | 0.58± 0.04 | 0.52 ± 0.04 |

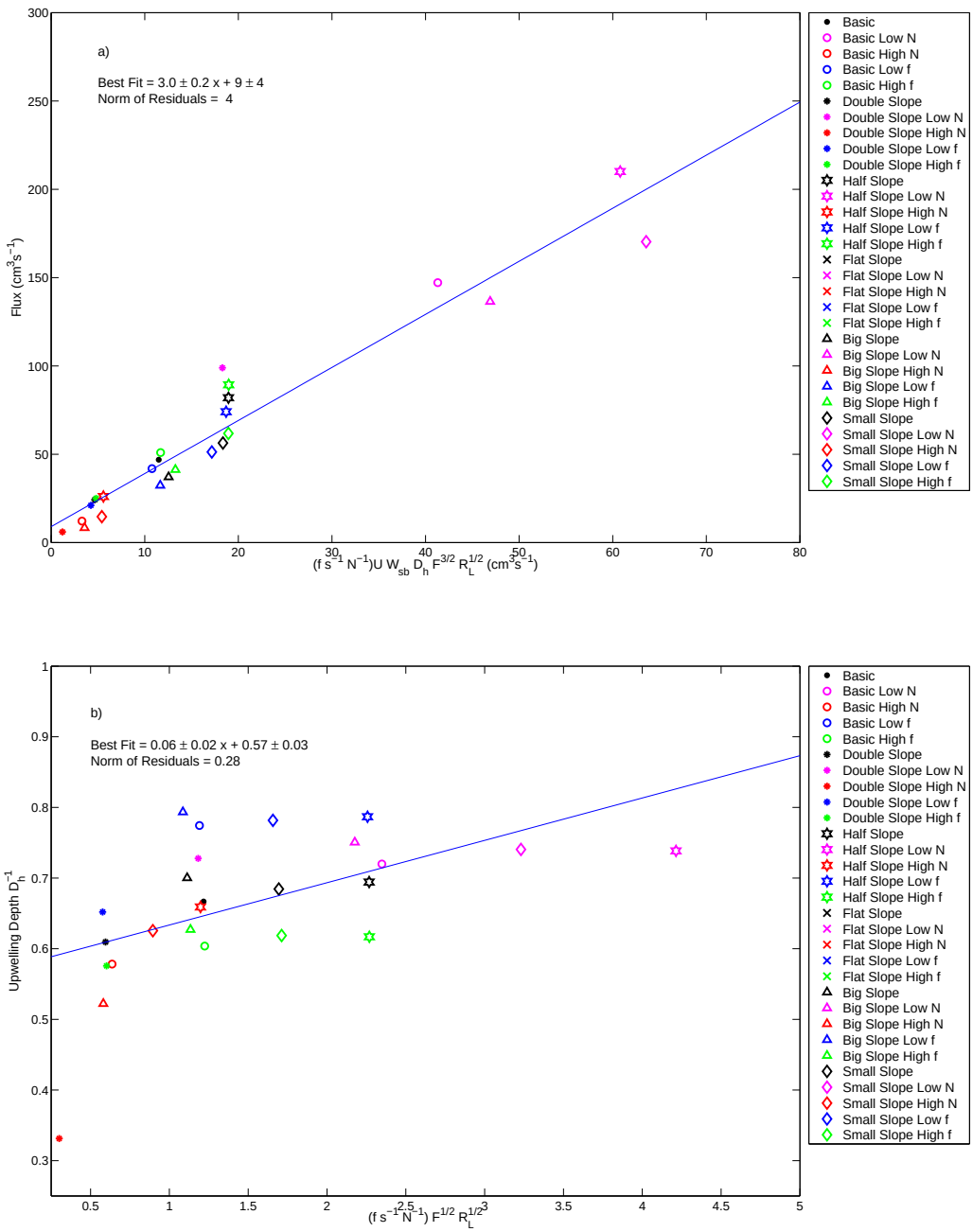


Figure 11: Observed versus scaled plots for a) a good linear relation between the scaled and observed upwelling flux using $f/(sN)$ to account for the slope. b) shows the scaled and observed upwelling depth using the same non-dimensional number used to produce a linear flux plot. The lines of best fit and the norm of residuals were found without using the flat slope cases. The norm of residuals is normalized to the x-axis.

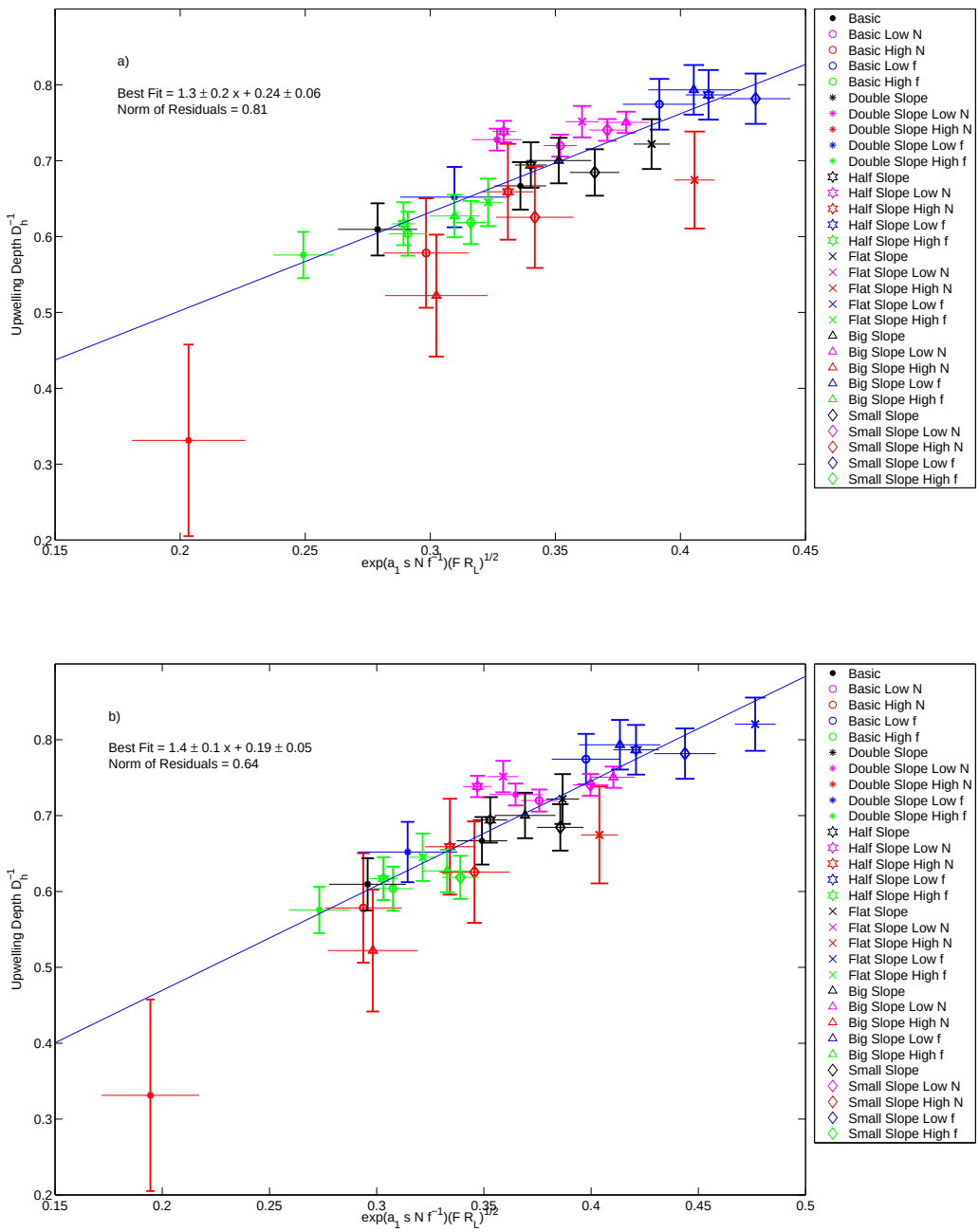


Figure 12: Observed versus scaled plots for the upwelling depth using the non-dimensional number to account for the effect of the shelf slope. a) Shows the result using a Rossy number based on the radius of curvature ($Ro = U/fR$) and b) shows the result using a Rossby number based on the canyon width ($Ro = U/fW$). The norm of residuals is normalized to the x-axis.

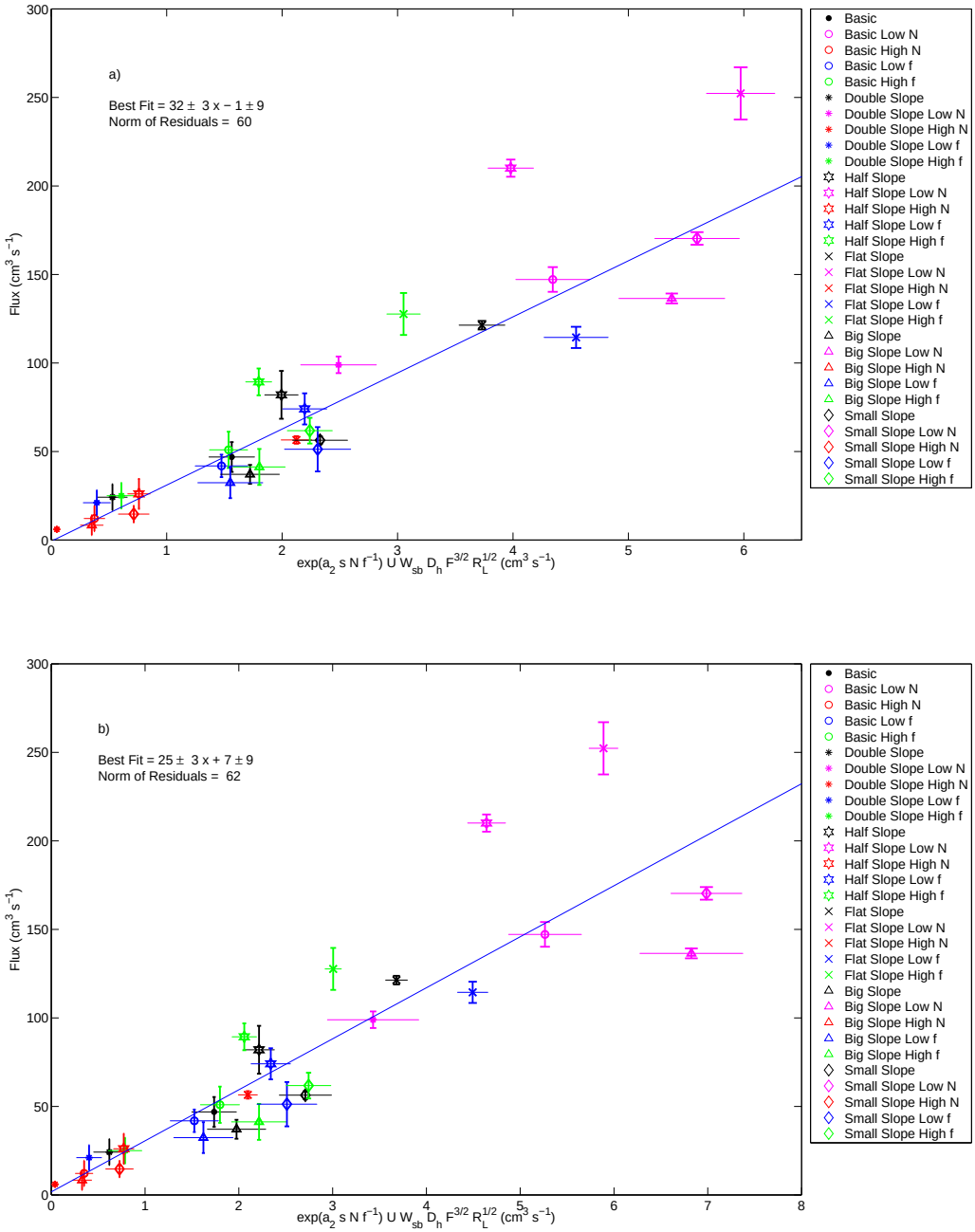


Figure 13: Observed versus scaled plots for the upwelling flux using the non-dimensional number to account for the effect of the shelf slope. a) Shows the result using a Rossy number based on the radius of curvature ($Ro = U/fR$) and b) shows the result using a Rossby number based on the canyon width ($Ro = U/fW$). The norm of residuals is normalized to the x-axis.

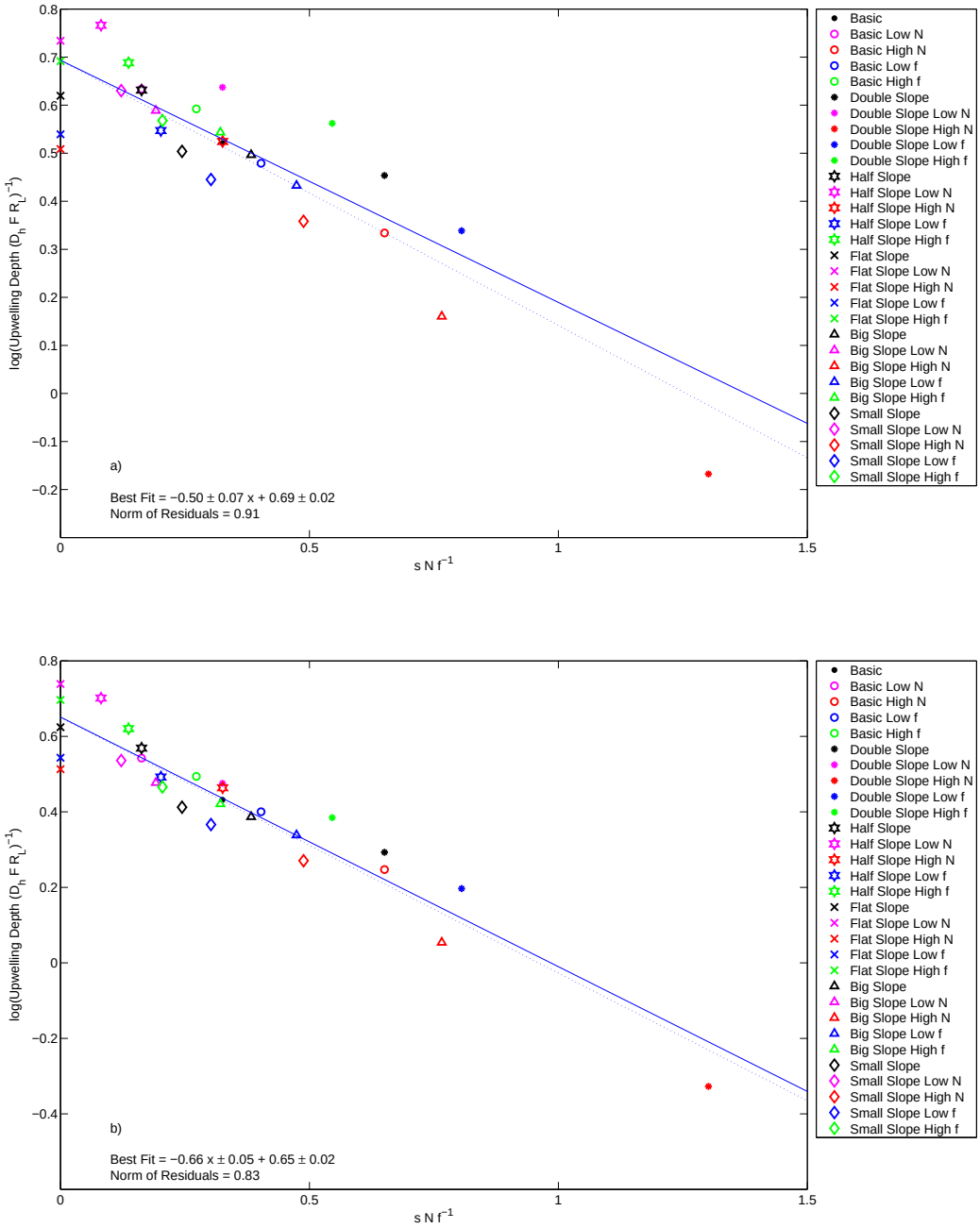


Figure 14: Linearized observed and scaled upwelling depth plots where a) Shows the result using a Rossy number based on the radius of curvature ($Ro = U/fR$) and b) shows the result using a Rossby number based on the canyon width ($Ro = U/fW$). The dotted line is a line of best fit using all points weighted equally. The solid line is a weighted line of best fit, where smaller error bars in Figure 12 are weighted more than those with larger error bars. The slopes of the weighted lines gives the values for $a_1$ for each Rossby number. The norm of residuals is normalized to the y-axis.

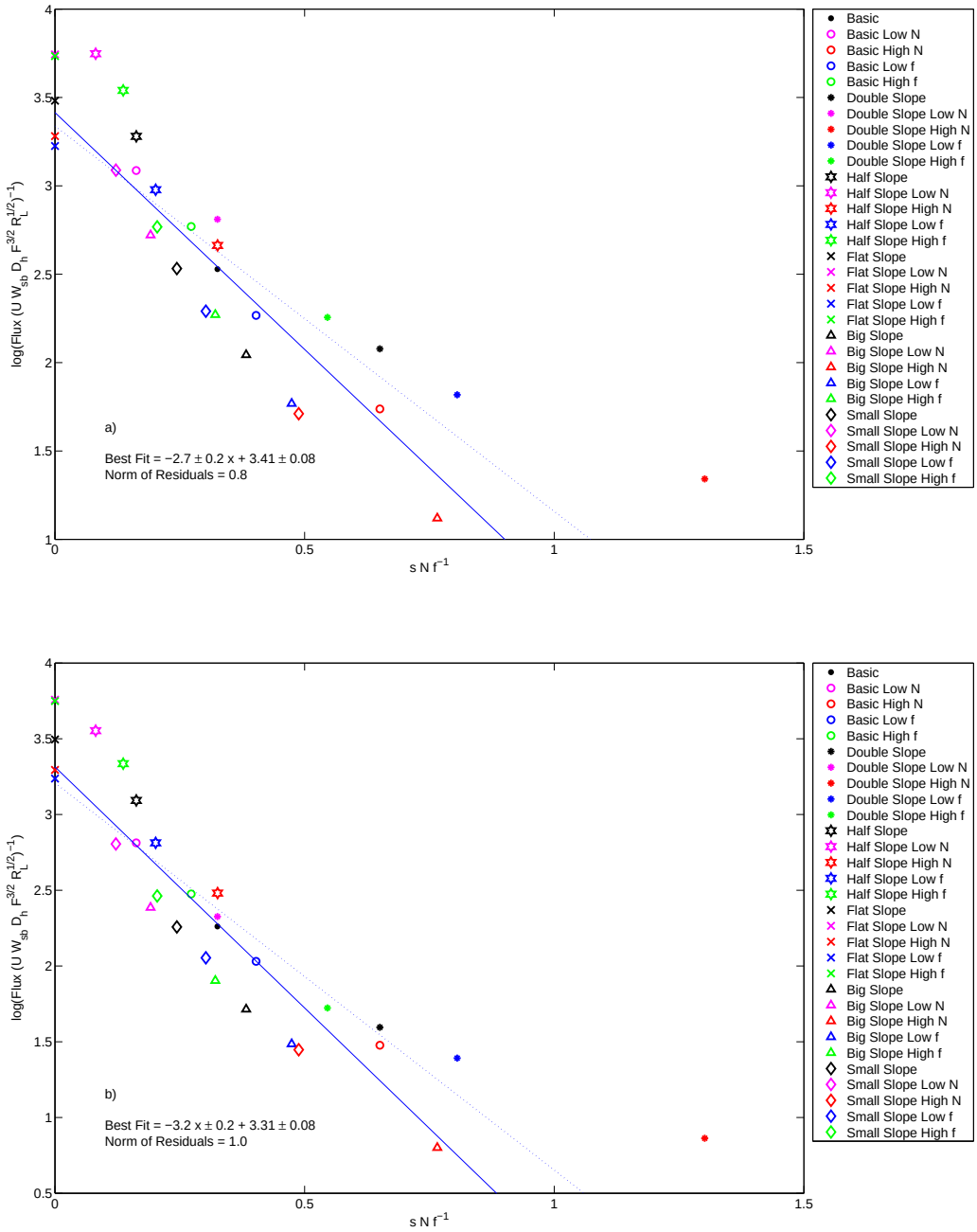


Figure 15: Linearized observed and scaled upwelling flux plots where a) Shows the result using a Rossy number based on the radius of curvature ($Ro = U/fR$) and b) shows the result using a Rossby number based on the canyon width ($Ro = U/fW$). The dotted line is a line of best fit using all points weighted equally. The solid line is a weighted line of best fit, where smaller error bars in Figure 13 are weighted more than those with larger error bars. The slopes of the weighted lines gives the values for $a_2$ for each Rossby number. The norm of residuals is normalized to the y-axis.

Table 4: This table shows the values for the coefficients $a_1$ and $a_2$ with corresponding error for both the upwelling depth and upwelling flux, respectively, using scales based on the radius of curvature, $R$, or the canyon width, $W$.

| | $a_1$ | $a_2$ |
|---|---|---|
| $Ro(R)$ | -0.50 ± 0.07 | -2.7 ± 0.2 |
| $Ro(W)$ | -0.66± 0.05 | -3.2 ± 0.2 |

Where $y = Z/D_h$, $Z$ is the depth of upwelling and $D_h$ is a depth scale defined earlier. $\sigma$ is referring to the error in each of its subscripts.

Since $Z$ was found by taking the difference between the deepest water on the shelf at head depth $(Z + H_h)$and the head depth $(H_h)$ the error in the measured depth of upwelling was determined by:

$$\sigma_Z = \sqrt{\sigma_{H_h}^2 + \sigma_{H_h+Z}^2} \tag{14}$$

Where $\sigma_{H_h}$ and $\sigma_{H_h+Z}$ are the errors in the $z$ direction. These are found by taking half of the $z$ grid spacing defined in the model.

Error in the depth scale $D_h$ was calculated as:

$$\sigma_{D_h} = \frac{f}{N}\sigma_L \tag{15}$$

Where $\sigma_L$ is the error in the length of the canyon. This was determined by taking half of the difference in the allowable canyon lengths determined from the minimum and maximum acceptable head depths.

The fractional error in the scaled normalized upwelling depth on the x-axes $(FR_L)^{1/2}$ for Figures 1a and 6a was determined to be:

$$\frac{\sigma_x}{x} = \sqrt{\frac{\sigma_F^2}{4F^2} + \frac{\sigma_{R_L}^2}{4R_L^2}} \tag{16}$$

Where $x = (FR_L)^{1/2}$, $F$ is a function of $Ro$ $(c_1 Ro/(c_2+Ro))$, and $R_L$ is a Rossby number.

But for Figure 12 where the x-axis is $\exp(a_1 sN/f)(FR_L)^{1/2}$ the fractional error was calculated as:

$$\frac{\sigma_x}{x} = \sqrt{\frac{\sigma_F^2}{4F^2} + \frac{\sigma_{R_L}^2}{4R_L^2} + \frac{\sigma_{a_1}^2 N^2 s^2}{f^2} + \frac{\sigma_s^2 N^2 a_1^2}{f^2}} \tag{17}$$

Where $x = \exp(asN/f)(FR_L)^{1/2}$, $s$ is the shelf slope, and $a_1$ is a coefficient described

earlier.

The fractional error in $F$ was calculated as:

$$\frac{\sigma_F}{F} = \frac{\sigma_{Ro}}{Ro}\left(\frac{c_2 + Ro - 1}{c_2 + Ro}\right) \tag{18}$$

Where $c_2 = 0.9$ and is a constant [*Allen and Hickey*, 2010].

The fractional error in $Ro$ was calculated as:

$$\frac{\sigma_{Ro}}{Ro} = \sqrt{\frac{\sigma_U^2}{U^2} + \frac{\sigma_R^2}{R^2}} \tag{19}$$

Where $U$ is the velocity upstream of the canyon and $R$ is the radius of curvature of the canyon.

The error in $U$ was found by taking half of the largest difference of the velocity at three locations upstream of the canyon at a depth of 1 cm; this value was found to be 0.02 cm/s.

Since $R$ was determined by using the Levenberg-Marquandt algorithm for non-linear least-squares curve fitting, the error in $R$ was determined by the difference in the solutions by using different lengths for which the solution was found. The difference between the solutions was approximately 0.2 cm.

In the cases where the Rossby number was found using the width of the canyon rather than the radius of curvature, $W$ would be used instead of $R$. The error in $W$ was determined by taking half the difference in the widths for the maximum and minimum allowable canyon lengths.

Error in the shelf slope, $s$, was calculated as:

$$\sigma_s = \sqrt{\sigma_{\Delta z}^2\left(\frac{1}{\Delta r}\right)^2 + \sigma_{\Delta r}^2\left(\frac{\Delta z}{\Delta r}\right)^2} \tag{20}$$

Where $\Delta z$ is the difference between the depth at the wall of the tank and the depth near the shelf break at 1.7 cm where the shelf has a linear slope within error, $\Delta r$ is the difference in radius between the same points as $\Delta z$.

The error $\sigma_{\Delta z}$ and $\sigma_{\Delta r}$ are found by $\sqrt{2\sigma_z^2}$ and $\sqrt{2\sigma_z^2}$ respectively where the error in $z$ and $r$ is half of the grid spacing.

Error in $a_1$ was returned in the least-squares solution to the slope of the weighted line of best fit in Figure 14.

### 6.3.2 Error in the Upwelling Flux

The error for the upwelling flux calculated from the model on the y-axis of Figures 1b, 6b, and 13 is found by calculating the flux between 29 s and 30 s and taking the difference from the flux value used over 25 s to 30 s.

The fractional error in the scaled flux used in Figures 1b and 6b was calculated as:

$$\frac{\sigma_\Phi}{\Phi} = \sqrt{\frac{\sigma_U^2}{U^2} + \frac{\sigma_{W_{sb}}^2}{W_{sb}^2} + \frac{\sigma_{D_h}^2}{D_h^2} + \frac{9\sigma_F^2}{4F^2} + \frac{\sigma_{R_L}^2}{4{R_L}^2}} \tag{21}$$

Where $\Phi$ is the upwelling flux and $W_{sb}$ is the width of the canyon at the shelf-break.

The error in $W_{sb}$ is found by taking half of the difference between the maximum and minimum acceptable values.

The fractional error for the upwelling flux using $\Phi = \exp(a_2 Ns/f)(UW_{sb}D_h)F^{3/2}R_L^{1/2}$ was calculated as:

$$\frac{\sigma_\Phi}{\Phi} = \sqrt{\frac{\sigma_U^2}{U^2} + \frac{\sigma_{W_{sb}}^2}{W_{sb}^2} + \frac{\sigma_{D_h}^2}{D_h^2} + \frac{9\sigma_F^2}{4F^2} + \frac{\sigma_{R_L}^2}{4{R_L}^2} + \frac{\sigma_{a_2}^2 N^2 s^2}{f^2} + \frac{\sigma_s^2 N^2 a_2^2}{f^2}} \tag{22}$$

Where $a_2$ is the analogous to the $a_1$ coefficient but for the upwelling flux rather than the depth of upwelling.

### 6.3.3 Error in Topographic Burger Number and $\beta^{-1}$

Error in the topographic Burger number $(sN/f)$ was calculated as:

$$\sigma_{sN/f} = \sigma_s \frac{N}{f} \tag{23}$$

The error in the non-dimensional number $\beta^{-1} = \exp(asN/f)$ included in the scaling was calculated as:

$$\sigma_{\beta^{-1}} = \sqrt{\frac{\sigma_a^2 N^2 s^2}{f^2} \exp\left(\frac{2asN}{f}\right) + \frac{\sigma_s^2 a^2 N^2}{f^2} \exp\left(\frac{2asN}{f}\right)} \tag{24}$$

Where the $a$ and it's corresponding error can be either $a_1$ or $a_2$.

# 7 Discussion

## 7.1 Assumptions

An assumption for the initial scaling by *Allen and Hickey* [2010] is that the slope is slightly sloped. This thesis tried to remove this assumption and allow the scaling of the upwelling depth and flux to be applicable to variations in shelf slope.

A non-dimensional number, $\beta$, was found that characterized the back pressure which becomes present with increasing slope. This number when incorporated into the scaling and rearranged acts to shallow the depth of upwelling and lower the upwelling flux with increasing slope by a factor of $\exp(asN/f)$.

There are some benefits to using an exponential: this also allows the slope to be used in such a way that if the slope were flat (equal to zero) then the $\beta$ term would be equal to one and there would be no added back pressure to the upwelling flow. And if there were any slope $\beta$ would increase representing the added back pressure to upwelling flow and restricting its movement further up the shelf.

An assumption here is that the slope of the shelf is positive, further tests would have to be done to see what would happen if the slope declined after the head of the canyon towards the coast. The dense water will likely flow down the slope which may pull the water behind it and acting to reduce the acting pressure.

This new scaling will still follow other assumptions by *Allen and Hickey* [2010] described earlier.

## 7.2 Slope Effect on Upwelling Characteristics

### 7.2.1 Depth of Upwelling

The depth of upwelling is greatly affected by the slope which can be seen by the separation of the points along the observed axis in Figure 6a for cases with the same slope, Coriolis, and most stratification cases. For example: with a Coriolis parameter of $f$=0.52 s$^{-1}$ and a buoyancy frequency of $N$=2.2 s$^{-1}$ a flat slope will have a greater upwelling depth and flux than a double slope case. It can be seen that the stratification can be low enough that the slope has no or little effect on the depth of upwelling as all low stratification cases have approximately the same depth of upwelling.

The low stratification will have a large upwelling depth that is independent of the shelf slope. This can be thought of the less dense water on the shelf is creating little

back pressure and thus there is little restriction of the upwelling. However, this is not observed in the scaled values (Figure 12) where the slope effect on stratification is clearly observed.

The high stratification cases on the other hand have a steeper slope than the line of best fit in Figure 6a which shows that the slope effect is greater than the stratification effect for denser water. The combination of a steep slope and very dense water will produce a larger back pressure and further restrict the water from being upwelled onto the shelf.

#### 7.2.2 Upwelling Flux

In comparison to the depth of upwelling the upwelling flux seems to have the opposite effect where the low stratification cases have a greater variation in flux with slope and the high stratification cases have a smaller variation with changing slope. This could be due to the back pressure of the water already on the shelf.

The slopes of the lines in Figure 8 for volume of water on the shelf are much steeper for the low stratification cases than the high stratification cases and so the flux will also be higher. Within the slope cases the slope of lines vary more for the low stratification and thus there will be a greater variation in flux. The slopes of the lines for the high stratification cases are more similar and thus the flux for each of these will be more similar.

Less dense water will result in a lower back pressure because the weight of the water on the shelf would be less. This makes it easier for the water push past itself with a steeper slope allowing the volume of water making it onto the shelf in the last five seconds of the model run time higher than what would have been present at earlier times. In this case the weight of the water has little effect on restricting movement further up the slope and so it is the shelf slope that is the key factor in limiting the rate at which the water arrives on the shelf.

The more dense the water the larger back pressure because the weight of the water on the shelf is larger. With a stronger stratification the heavier water has a greater momentum to push past the less dense water already on the shelf; therefore, changes in the shelf slope have little effect on the rate that the dense water can make it onto the shelf and the fluxes would be similar.

## 7.3 Scales

### 7.3.1 Depth of Upwelling Scales

The scaling for the depth of upwelling with the included non-dimensional term to account for the shelf slope shows a good relationship with the observed upwelling depth. This can be seen by the low norm of residuals (Figure 12). These figures also show that the scale works best using a Rossby number as a function of the canyon width, $W$, because it has a lower norm of residuals compared to the scale using a Rossby number as a function of the radius of curvature, $R$. This means the width of the canyon determines whether flow crosses the canyon and drives upwelling rather than following the isobaths. The two results have a percent difference of about 23% in the norm of residuals. This is a different relation than that posed by *Allen and Hickey* [2010], who say the radius of curvature, $R$, will determine whether there is upwelling.

### 7.3.2 Upwelling Flux Scales

The scaling for the upwelling flux with the included non-dimensional term to account for the shelf slope shows a good relationship with the observed upwelling flux; however, the low stratification cases are still very scattered. This can be seen by the low norm of residuals (Figure 13). These figures also show that the scale works best using a Rossby number as a function of the radius of curvature, $R$, because it has a lower norm of residuals compared to the scale using a Rossby number as a function of the canyon width, $W$. This means that the radius of curvature, $R$, determines whether the flow will cross the canyon rather than follow the isobaths. The two results have a percent difference of about 3% in the norm of residuals. This agrees with *Allen and Hickey* [2010] but not with the depth of upwelling in this study.

Since the percent difference is very small in this case more work would have to be done either by re-analyzing the statistics or looking at more canyons to confirm whether it is $R$ or $W$ that determines if the flow will cross the canyon. Since the two results are very close it is possible that the canyon width could be that determining factor.

# 8 Conclusions

A previous investigation into the accuracy of the scaling developed by *Allen and Hickey* [2010] showed that the shelf slope has an impact on the upwelling depth and flux

for flow over submarine canyons. This thesis investigated how the shelf slope plays a role in the upwelling over submarine canyons by creating a non-dimensional number which takes into account the shelf slope. This number is incorporated into the scaling by acting as a back pressure to the flow reaching the shelf. As water piles up on the shelf this creates a back pressure restricting water from moving up the shelf. The effect of the back pressure on the depth of upwelling and upwelling flux was found to be $\exp(asN/f)$.

A comparison of Rossby numbers used in the scaling show that the radius of curvature, $R$, has a better fit with the data for the depth of upwelling, but the canyon width, $W$ has a better fit with the data for the upwelling flux.

Future research will include looking for a more physical explanation of why an exponential term works for the scaling or whether it is some other function of $sN/f$. Also further research should look into whether the canyon width or radius of curvature determines whether the flow will follow the isobaths or cross the canyon and drive the upwelling. This was only one experiment and the two theories of 1) $\exp(asN/f)$ characterizes the back pressure and 2) that it is likely the width of the canyon determines whether the flow follows the isobaths or crosses them to flow over the canyon and drive upwelling should be tested with other canyon geometries and with real-world canyons.

# References


Allen, S. E., 1996: Topographically generated, subinertial flows within a finite length canyon. *J. Phys. Oceanogr.*, **26**, 1608–1632.

Allen, S. E., 2004: Restrictions on deep flow across the shelf-break and the role of submarine canyons in facilitating such flow. *Surv. Geophys.*, **25**, 221–247.

Allen, S. E. and X. Durrieu de Madron, 2009: A review of the role of submarine canyons in deep-ocean exchange with the shelf. *Ocean Sci.*, **5**, 607–620.

Allen, S. E. and B. M. Hickey, 2010: Dynamics of advection-driven upwelling over a shelf break submarine canyon. *J. Geophys. Res.*, **115**, C08 018.

Allen, S. E., C. Vindeirinho, R. E. Thomson, M. G. G. Foreman, and D. L. Mackas, 2001: Physical and biological processes over a submarine canyon during an upwelling event. *Can. J. Fish. Aquat. Sci.*, **58**, 671–684.

Bevington, P. R., 1969: *Data Reduction and Error Analysis for the Physical Sciences.* McGraw-Hill Book Company, 56-65 pp.

Brink, K. H. and S. J. Lentz, 2010: Buoyancy arrest and bottom ekman transport. part I: Steady flow. *J. Phys. Oceanogr.*, **40**, 621–635.

Dawe, J. T. and S. E. Allen, 2010: Solution convergence of flow over steep topography in a numerical model of canyon upwelling. *J. Geophys. Res.*, **115**, C05 008.

Freeland, H. J. and K. L. Denman, 1982: A topographically controlled upwelling center off southern vancouver island. *J. Mar. Res.*, **40**, 1069–1093.

Holton, J. R., 1992: *An Introduction to Dynamic Meteorology.* 3d ed., Academic Press, 511 pp.

Jacox, M. G. and C. A. Edwards, 2011: Effects of stratification and shelf slope on nutrient supply in coastal upwelling regions. *J. Geophys. Res.*, **116**, C03 019.

Kämpf, J., 2010: On preconditioning of coastal upwelling in the eastern great australian bight. *J. Geophys. Res.*, **115**, C12 071.

Lentz, S. J. and D. C. Chapman, 2004: The importance of nonlinear cross-shelf momentum flux during wind-driven coastal upwelling. *J. Phys. Oceanogr.*, **34**, 2444–2457.

Marshall, J., A. Adcroft, C. Hill, L. Perelman, and C. Heisey, 1997: A finite-volume, incompressible Navier Stokes model for studies of the ocean on parallel computers. *J. Geophys. Res.*, **102**, 5753–5766.

Nof, D., 1982: The translation of isolated cold eddies on a sloping bottom. *Deep-Sea Research*, **30**, 171–182.

# Appendices

## A Initial Scaling

This is the scaling for upwelling over submarine canyons developed by *Allen and Hickey* [2010].

The scaling is based on the advection-driven upwelling and is assumed to be steady. The shallow water equations for steady, inviscid, stratified flow with Boussinesq, incompressible and non-diffusive approximations are:

$$\overrightarrow{u} \cdot \nabla \overrightarrow{u} - f\hat{k} \times \overrightarrow{u} = \frac{-1}{\rho_o} \nabla p \tag{25a}$$

$$\nabla \cdot \overrightarrow{u} = 0 \tag{25b}$$

$$\overrightarrow{u} \cdot \nabla \rho = 0 \tag{25c}$$

$$\frac{\partial p}{\partial z} = \rho g \tag{25d}$$

where $\overrightarrow{u}$ is the horizontal velocity, $f$ is the Coriolis parameter, $\hat{k}$ is the vertical unit vector, $\rho_o$ is a constant reference density, $p$ is the pressure, and $g$ is the gravitational acceleration.

### A.1 Depth of Upwelling

Using equation (25a) in polar coordinates it is possible to find the pressure change along the canyon that drives the upwelling.

$$u_r \frac{\partial u_\theta}{\partial r} + \frac{u_\theta}{r} \frac{\partial u_\theta}{\partial \theta} + \frac{u_\theta u_r}{r} + f u_r = \frac{-1}{\rho_o r} \frac{\partial p}{\partial \theta} \tag{26}$$

The first term of this equation is small compared to the third term and can be neglected. By conservation of volume the second term can be written as:

$$u_\theta \frac{1}{r} \frac{\partial u_\theta}{\partial \theta} = u_\theta \left( -\frac{\partial w}{\partial z} - \frac{\partial u_r}{\partial r} \right) \tag{27}$$

Where $\partial w / \partial z$ is small in comparison to $\partial u_r / \partial r$ and will also be neglected. The second term of equation (26) can then be scaled as $UV/R$, where $R$ is the radius of curvature of

the canyon (Figure 3). The third term can be scaled as $UV/R$, $fu_r$ can be scaled as $fV$. A function $F$ is defined as a function of the Rossby number ($Ro = U/fR$) which turns along-isobath flow into cross-isobath flow, so $V = F(Ro)U$ and

$$F(Ro) = \frac{c_1 Ro}{c_2 + Ro} \tag{28}$$

Where $c_1$ and $c_2$ are constants.

Now rearranging the scaled equation (26) becomes:

$$-\rho_o fUF = \frac{1}{r}\frac{\partial p}{\partial \theta} \tag{29}$$

This is the pressure gradient along the upstream rim edge of the canyon.

The pressure difference between the head and the mouth of the canyon (equation 30) is the pressure gradient multiplied by a length scale, $L$. Here the length scale is defined as the distance between the mouth at the shelf-break depth and the head of the canyon which is determined by the last dimpled isobath of the canyon ($L$ in Figure 3).

$$-\rho_o fUFL = L\frac{\partial p}{\partial \theta} \tag{30}$$

Now to determine the deformation of the density field, which will allow the depth of upwelling to be determined, equations (25) are rewritten using the natural coordinate system [e.g. *Holton*, 1992]:

$$u\frac{\partial u}{\partial s} = \frac{-1}{\rho_o}\frac{\partial p}{\partial s} \tag{31a}$$

$$\frac{u^2}{R'} + fu = \frac{-1}{\rho_o}\frac{\partial p}{\partial n} \tag{31b}$$

$$\frac{\partial u}{\partial s} + \frac{\partial w}{\partial z} = 0 \tag{31c}$$

$$u\frac{\partial p}{\partial s} + w\frac{\partial p}{\partial z} = 0 \tag{31d}$$

$$\frac{\partial p}{\partial z} = -\rho g \tag{31e}$$

Where $u$ is the velocity following the horizontal direction of flow, $s$; $w$ is the vertical velocity; $\rho$ is the density field; and $R'$ is the radius of curvature of the streamlines.

The deepest streamline to cross the rim of the canyon is found to be at a depth $Z + H_s$ where $Z$ is the upwelling depth and $H_s$ is the depth of the shelf break. Along this

streamline the density is conserved, which is given in equation (31d). Scaling equation (31d) gives:

$$\frac{U_*\Gamma}{L} - \frac{\Omega\rho_o N^2}{g} = 0 \tag{32}$$

Where $U_*$ is the velocity of the upwelling stream, $\Gamma$ is the scale of horizontal density perturbations, $L$ is a length scale from the shelf-break to the head of the canyon, and $\Omega$ is the vertical velocity scale.

Scaling the conservation of mass equation (31c) gives:

$$\frac{U_*}{L} - \frac{\Omega}{Z} = 0 \tag{33}$$

Where $Z$ is the depth of upwelling.

Since the pressure change along the canyon that drives upwelling is in balance with the density gradient due to the perturbation density equation (31e) will be scaled as:

$$\frac{\rho_o fUFL}{Z} = \Gamma g \tag{34}$$

To find the scale for the depth of upwelling equations (32), (33), and (34) will be combined:

$$Z = D_h(FR_L)^{1/2} \tag{35}$$

Where $R_L$ is a Rossby number given by $R_L = U/fL$ and $D_h$ is a depth scale given by $D_h = fL/N$.

## A.2 Upwelling Flux

The scale for upwelling flux can be found by scaling equation (31b). This flow is found directly below the shelf-break flow crossing the canyon and has a scaled pressure gradient of $fUF$. At the lowest part of the upwelling stream at $Z$ there is no pressure gradient. Between the shelf-break and $Z$ the pressure gradient is half of that at the shelf-break, so the scaled pressure gradient of the upwelling stream is given by $(1/2)fUF$.

$$\frac{U_*^2}{W_{sb}} + fU_* = \frac{1}{2}fUF \tag{36}$$

Where $W_{sb}$ is the shelf-break width of the canyon and is the turning radius of the flow into the canyon. The first term is small and can be neglected [*Allen and Hickey*, 2010],

doing this equation (36) becomes:

$$U_* = \frac{1}{2}UF \tag{37}$$

The flux is found by, $\Phi = U_*$ multiplied by the area of upwelling stream. The area is found by the multiplication of the depth of upwelling, $Z$ and the shelf-break width, $W_{sb}$.

$$\Phi = U_* Z W_{sb} = (U W_{sb} D_H) F^{3/2} R_L^{1/2} \tag{38}$$